Observed trends in ground-level O_3 in Monterrey, Mexico during 1993-2014: Comparison with Mexico City and Guadalajara

Iván Y. Hernández Paniagua[1,2], Kevin C. Clemitshaw[3], and Alberto Mendoza[1,*]

[1]Escuela de Ingeniería y Ciencias, Tecnologico de Monterrey, Campus Monterrey, Av. Eugenio Garza Sada 2501, Monterrey, N.L., México, 64849.
[2]Centro de Ciencias de la Atmosfera, Universidad Nacional Autónoma de México, Circuito Exterior de Ciudad Universitaria, Ciudad de México, 04510, México
[3]Department of Earth Sciences, Royal Holloway University of London, Egham, Surrey TW20 0EX, UK.
*Corresponding author: mendoza.alberto@itesm.mx

Keywords
Air quality, emissions inventory, odd oxygen, time series, wind-sector analysis

Abstract
The largest urban areas in Mexico have experienced historically high ambient O_3 levels. Here, we present an assessment of long-term trends in O_3 and odd oxygen (O_3 + NO_2) at the industrial Monterrey metropolitan area (MMA) in NE Mexico. High-precision and high-frequency UV-photometric measurements of ambient O_3 have been made since 1993 at 5 sites within the MMA. Diurnal amplitudes in O_3 (AV_d) are used as a proxy for net O_3 production, which is influenced by the NO_2 photolysis rate. No significant differences are observed in the AV_d during weekdays when fossil fuel use and combustion process are higher than during weekends, although the largest AV_d are observed at sites downwind of industrial areas. During weekdays, cycle troughs and peaks are typically recorded at 07:00 and 14:00 CDT, respectively, and during weekends, at 06:00 and 13:00 CDT, respectively.

The O_3 annual cycle is driven by changes in meteorology and photochemistry, with maximum O_3 mixing ratios recorded in spring and minimum values in winter. The largest annual variations in O_3 are typically observed downwind of the MMA, with the lowest variations generally recorded in highly populated areas and close to industrial areas. A wind sector analysis shows that, at all sites, the highest O_3 mixing ratios are typically recorded from the E and SE sectors, while the lowest values are recorded in air masses from the W and NW. A wind sector analysis of mixing ratios of O_3 precursors revealed that the dominant sources of emissions are located in the industrial regions within the MMA and the surrounding area. Significant increasing trends in O_3 in spring, summer and autumn are observed depending on site location, with trends in annual averages ranging between 0.19 and 0.33 ppb yr^{-1}. The largest annual increases in O_3 are for the E and SE sectors, 0.50 and 0.66 ppb yr^{-1}, respectively. Overall, during 1993 to 2014, within the MMA, O_3 has increased at an average rate of 0.22 ppb yr^{-1} (p<0.01), which is in marked contrast with the decline of 1.15 ppb yr^{-1} (p<0.001) observed in the Mexico City metropolitan

area (MCMA) for the same period. No clear trend is observed during 1996 to 2014 within the Guadalajara metropolitan area (GMA).

1. Introduction

O_3 is a secondary air pollutant formed in the troposphere via the photo-oxidation of CO, methane (CH_4) and volatile organic compounds (VOCs) in the presence of NO and NO_2 ($NO + NO_2 = NO_X$) (Jenkin and Clemitshaw, 2000). The system of O_3 production is not linear, and is termed NO_x-limited, when O_3 production increases in response to increasing NO_X emissions, and termed VOC-limited when it responds positively to emissions of VOCs (Monks et al., 2015; Pusede et al., 2015). Tropospheric O_3 is of concern to policy makers due to its adverse impacts on human health, agricultural crops and vegetation, and also due to its role as a greenhouse gas despite its relatively short lifetime of around 22.3 ± 3.0 days (Stevenson et al., 2006; IPCC, 2013; WHO, 2014; Lelieveld et al., 2015). As the predominant source of OH, tropospheric O_3 controls the lifetime of CH_4, CO, VOCs, among many other air pollutants (Revell et al., 2015). In polluted regions, increased levels of O_3 are prevalent during seasons with stable high-pressure systems and intense photochemical processing of NO_X and VOCs (Dentener et al., 2005; Xu et al., 2008) with downward transport from the stratosphere of lesser importance (Wang et al., 2012). By contrast, the main removal processes for tropospheric O_3 are photochemical loss and dry deposition (Atkinson, 2000; Jenkin and Clemitshaw, 2000).

Tropospheric O_3 increased in the Northern Hemisphere (NH) during 1950-1980s due to rapid increases in precursor emissions during the industrialisation and economic growth of Europe and North America (NA) (Staehelin and Schmid, 1991; Guicherit and Roemer, 2000). Since the 1990s, reductions in O_3 precursor emissions in economically developed countries have resulted in decreases in tropospheric O_3 levels (Schultz and Rast, 2007; Butler et al., 2012; Pusede et al., 2012), however, in some regions, increases in O_3 have also been reported. For instance, from an analysis of O_3 data from 179 urban sites over France during 1999-2012, Sicard et al. (2016) reported an increasing trend in the annual averages of 0.14 ± 0.19 ppb yr^{-1}, and in the medians of 0.13 ± 0.22 ppb yr^{-1}, attributed to long-range transport and reduced O_3 titration by NO due to reductions in local NO_X emissions. However, Sicard et al. (2016) also reported during the same period that at 61 rural sites, O_3 decreased in the annual averages by 0.12 ± 0.21 ppb yr^{-1}, and in the medians by 0.09 ± 0.22 ppb yr^{-1}.

In the US and Canada, O_3 levels have decreased substantially at different metrics during the last two decades in response to more stringent emission controls focused on on-road and industrial sources. In the Greater Area of Toronto from 2000 to 2012, O_3 levels decreased at urban sites by approximately 0.4 % yr^{-1}, and at sub-urban sites by approximately 1.1 % yr^{-1}, as a consequence of a reduction in the mid-day averages of NO_2 of 5.8 - 6.4 % yr^{-1}, and in the VOC reactivity of 9.3% yr^{-1} (Pugliese et al., 2014). Emission estimates suggest an overall national scale decrease during 1980-2008 in US NO_X and VOCs emissions of 40 % and 47 %, respectively, with city-to-city varaiablity (EPA, 2009; Xing et al., 2013).

Lefohn et al. (2010) reported that for 12 US major metropolitan areas, the O_3 US EPA exposure metrics of the annual 2nd highest 1-h average, and the annual 4th highest daily maximum 8-h average, decreased during 1980-2008 at 87 % and 71 % of the monitoring sites evaluated, respectively. However, Lefohn et al. (2010) observed an increase in the lower- and mid-O_3 mixing ratios in response to decreased titration by NO. More recently, Simon et al. (2015) assessed changes in the 1-h average O_3 mixing ratios at around 1400 sites across the US between 1998-2013, using the 5th, 25th, 50th 75th 95th percentiles, and the maximum daily 8-h average. Overall, Simon et al. (2015) observed increases at the lower end of the O_3 data distribution of 0.1-1 ppb yr^{-1}, mostly in urban and sub-urban areas, whereas O_3 decreased at the upper end of the data distribution between 1-2 ppb yr^{-1} at less urbanised areas. Such changes were associated with the implementation of control strategies within the US to abate peak O_3 mixing ratios, as the NO_X SIP Call and, tighter point and vehicle emission standards.

In Mexico, studies of long-term trends in O_3 have focused on the Mexico City Metropolitan Area (MCMA) (Molina and Molina, 2004; Jaimes et al., 2012; Rodriguez et al., 2016), with reports of a decrease in O_3 annual averages of ca. 33 % during the last two decades (Parrish et al., 2011; SEDEMA, 2016a). O_3 has received less consideration at other large metropolitan areas, where Mexican air quality standards are frequently exceeded (Table 1). Indeed, since 2000, recorded O_3 mixing ratios have exceeded Mexican official standards for O_3 1-h average (110 ppb) and 8-h running average (80 ppb) by more than 50 % at the Guadalajara metropolitan area (GMA, the second most populated city) and at the Monterrey metropolitan area (MMA, the third most populated city (INE, 2011; SEMARNAT, 2015). To date, only Benítez-García et al. (2014) have addressed changes in ambient O_3 at the GMA and MMA during 2000-2011, reporting an increase in O_3 annual averages of around 47 % and 42 %, respectively. However, it should be noted that the ordinary linear regression analysis used by Benítez-García et al. (2014) may be biased by extreme values and is therefore not suitable to determine O_3 long-term trends with significant confidence.

To improve air quality, the Mexican government has introduced several initiatives to reduce primary pollutants emissions, with emission estimates reported in the Mexican National Emissions Inventories (NEI). The NEI suggest that from 1999 to 2008, anthropogenic NO_X emissions decreased at the MCMA by 3.8 % yr^{-1}, but increased at the GMA and the MMA by 1.9 % yr^{-1}, and by 4.0 % yr^{-1}, respectively (Fig. S1) (SEMARNAT, 2006, 2011, 2014). These NEI NO_X emission estimates agree with the decrease for the MCMA of 1.7 % yr^{-1} in the NO_2 vertical column density during 2005-2014 reported by Duncan et al. (2016), but disagree for the GMA and the MMA where decreases of 2.7 % yr^{-1} and of 0.3 % yr^{-1}, respectively, are reported. Similarly, Boersma et al. (2008) observed that NO_X emissions over Mexico derived from NO_2 satellite observations were higher by a factor of 1.5 - 2.5 times than bottom-up emission estimates, which were lower by 1.6 - 1.8 times than data reported in the NEI 1999-base year. The NEI anthropogenic VOCs emissions estimates suggest a decrease at the MMA by 0.2 % yr^{-1}, but increases at the MCMA and at the GMA by 2.7 % yr^{-1} and by 3.2 % yr^{-1}, respectively (Fig. S1) (SEMARNAT, 2006,

2011, 2014). However, as for NO_X, NEI trends in VOCs disagree with existing reports for average VOCs decreases within the MCMA (Arriaga-colina et al., 2004; Garzón et al., 2015).

Local authorities have developed local emission inventories for the MCMA and the MMA, although only for the MCMA the inventories have been compiled with a frequency of two years since 1996 (SEDEMA, 1999, 2001, 2003, 2004, 2006, 2008, 2010, 2012, 2014, 2016b; SDS, 2015). The accuracy of the MCMA emission inventories has been also assessed during several field campaigns. For instance, during the MCMA 2002-2003 campaign, Velasco et al. (2007) observed an overestimation in the 1998 inventory for VOCs emissions of alkenes and aromatics, but an underestimation in the contribution of some alkanes. By contrast, for the 2002 MCMA inventory, Lei et al. (2007) reported an underestimation in the VOCs total emissions of around 65 %, based on a simulation of an O_3 episode occurred in 2003 within the MCMA. Therefore, since these emission estimates are used to predict future air quality, and to design clean air policies, it is imperative to examine the results of the policies implemented to control emissions of O_3 precursors.

To our knowledge, no previous study has address trends in O_3 and odd oxygen in urban areas of Mexico. In this study, we describe trends in ground-level O_3 within the MMA, and its response to changes in precursor emissions during 1993-2014. Long-term and high-frequency measurements of O_3 were recorded at 5 air quality monitoring stations evenly distributed within the MMA. In order to better assess photo-chemical production of O_3, odd oxygen defined as ($[O_X] = [O_3] + [NO_2]$) was also considered, as O_3 and NO_2 are rapidly interconverted. Diurnal and annual cycles of O_3 and O_X are used to interpret net O_3 production within the MMA. We show that air mass origin influences strongly the O_3 annual growth rates. The trends in O_3, O_X and precursor emissions are compared with those observed within the MCMA and GMA. Finally, we describe that NEI emission estimates for NO_X and VOCs disagree in the trend magnitudes with ground-based NO_X and VOCs measurements made at the urban areas studied here.

This paper is organised as follows: Section 2 presents the data quality and methodology used to derived the different trends presented. Section 3 describes in detail the O_3 and O_X diurnal and annual cycles, and, annual and seasonally averaged trends. Section 4 discusses the origin of the O_3 and O_X diurnal variations and trends in the light of changes in precursor emissions. Finally, Section 5 provides some conclusions regarding the trends observed at the studied urban areas.

2. Methodology

2.1 Monitoring of O_3 in the Monterrey Metropolitan Area (MMA).

The MMA (25°40'N, 100°20'W) is located around 720 km N of Mexico City, some 230 km S of the US border in the State of Nuevo Leon (Fig. 1a). It lies at an average altitude of 500 m above sea level (m asl) and is surrounded by mountains to the S and W, with flat terrain to the NE (Fig. 1b). The MMA is the largest urban area in Northern Mexico at around 4,030 km^2, and is the third most populous in the country

with 4.16 million inhabitants, which in 2010, comprised 88 % of the population of Nuevo Leon State (INEGI, 2010). It is the second most important industrial area in Mexico and has the highest gross domestic product per capita (Fig. 1c). Although the weather changes rapidly on a daily time-scale, the climate is semi-arid with an annual average rainfall of 590 mm, and an annual average temperature of 25.0°C with hot summers and mild winters (ProAire-AMM, 2008; SMN, 2016).

Within the MMA, tropospheric O_3, 6 additional air pollutants (CO, NO, NO_2, SO_2, PM_{10}, and $PM_{2.5}$) and 7 meteorological parameters (wind speed (WS), wind direction (WD), temperature (Temp), rainfall, solar radiation (SR), relative humidity (RH) and pressure) have been monitored continuously, with data summarised as hourly averages, since November 1992 at 5 stations that form part of the Integral Environmental Monitoring System (SIMA) of the Nuevo Leon State Government (Table 2; SDS, 2016). From November 1992 to April 2003, and in accordance with EPA, EQOA-0880-047, Thermo Environmental Inc. (TEI) model 49 UV photometric analysers were used to measure O_3 with stated precision less than ±2 ppb O_3 and a detection limit of 2 ppb O_3. Similarly, in accordance with RFNA-1289-074, TEI model 42 NO-O_3 chemiluminescence detectors were used to measure NO-NO_2-NO_x with stated precision less than ±0.5 ppb NO, and a detection limit of 0.5 ppb NO. In May 2003, replacement TEI model 49C O_3 and model 42C NO-NO_2-NO_x analysers were operated as above, with stated precision better than ±1 ppb O_3 and ±0.4 ppb NO, respectively, and detection limits of 1 ppb O_3 and 0.4 ppb NO, respectively. To rule out instrumentation influences on the determined air pollutants trends, long-term trends based on annual averages were compared with those derived using 3-yr running averages, in accordance with Parrish et al. (2011) and Akimoto et al. (2015) (Supplementary Information S1.1; Fig. S2). Calibration, maintenance procedures and quality assurance/quality control (QA/QC) followed protocols established in the Mexican standards NOM-036-SEMARNAT-1993 and NOM-156-SEMARNAT-2012. The SIMA dataset has been validated by the Research Division of Air Quality of the Secretariat of Environment and Natural Resources (SEMARNAT). The monitoring of O_3 and other air pollutants at the MCMA and the GMA is detailed in the Supplementary Information S1.2-3.

2.2 NEI data

NEI data for estimated NO_x and VOCs emissions for the 1999-, 2005- and 2008-base years were obtained from the SEMARNAT website (http://sinea.semarnat.gob.mx). The data comprised emission sources (mobile, point, area and natural) and air pollutants (NO_X, VOCs, SO_X, CO, $PM_{2.5}$ and PM_{10}), at national, state and municipality scales. The NEI emission estimates are developed in accordance with the Manual for the Emission Inventories Program of Mexico (Radian, 2000), which is based on the US EPA AP-42 emission factors categorisation (EPA, 1995). The emission factors are regionalised for each Mexican state, based upon on-site measurements and survey information. Updates to the emission factors have been conducted for each released NEI, although no changes in the methodology were implemented between the 1999- and 2008-base years. Overall, the mobile emissions were estimated using the MOBILE6-Mexico model (EPA, 2003). The emissions from point sources were derived using

the annual operation reports submitted to the Environment Ministry. The emissions from area sources were obtained using the categorisation of Mexican area sources and the regionalised AP-42 emission factors.

The MCMA emissions inventories have been developed with a 2-year frequency since 1996, and were obtained from the MCMA Environment Secretariat website (http://www.aire.cdmx.gob.mx/). The methodology used to construct the MCMA inventories estimates is consistent with that used in the NEI (SEDEMA, 2016a), which is based on the AP-42 EPA emission factors. However, more speciated emission factors have been developed in each released version, considering updates in the local industrial activity, survey information and field measurement campaigns. To date, the only significant change in the methodology is the replacement of the Mobile6-Mexico model with the MOVES model to obtain the 2014-base year mobile emissions (SEDEMA, 2016b). As for the MCMA inventories, more speciated emission factors than those contained in the NEI were developed to produce the MMA emissions inventory 2013-base year (SDS, 2015), although, mobile emissions estimates were obtained with the Mobile6-Mexico model (EPA, 2003).

2.3 Analytical methods

SIMA, SIMAT (Atmospheric Monitoring System of the MCMA) and SIMAJ (Atmospheric Monitoring System of the GMA) instrumentation recorded O_3 data every minute, which were then validated and archived as 1-h averages. Total SIMA O_3 data capture by year and site are shown in Fig. S3. Data capture averaged during 1993-2014 ranged from 82.6 % at GPE to 93.3 % at SNB, with data capture <50 % during 1998-2000 at GPE, in 1998 at SNN, and in 1999 at OBI. A threshold of 75% data capture was defined to consider data valid and representative (ProAire-MMA, 2008; Zellweger et al., 2009; Wilson et al., 2012). All data were processed with hourly averages used to determine daily averages, which were used to calculate monthly averages, from which yearly averages were obtained.

2.4 Data analysis methods

The SIMA, SIMAT and SIMAJ O_3 data sets were analysed extensively using the *openair* package v. 1.1-4 (Carslaw and Ropkins, 2012) for R software v. 3.1.2 (R Core Team, 2013). In this study, the *openair* functions windRose, timeVariation and TheilSen were used to analyse air pollution data. Briefly, the windRose summarises wind speed and wind direction by a given time-scale, with proportional paddles representing the percentage of wind occurrence from a certain angle and speed range. The timeVariation function was used to obtain normalised daily cycles by season, and weekly cycles, with the 95 % confidence intervals in the cycles calculated from bootstrap re-sampling, which accounts for better estimations for non-normally distributed data (Carslaw, 2015). Finally, long-term trends of air pollutants at the MCMA, GMA and MMA were computed with the TheilSen function, which is based on the non-parametric Theil-Sen method (Carslaw, 2015; and references therein). The Theil-Sen estimate of the slope is the median of all slopes calculated for a given n number of x,y pairs, while the regression

parameters, confidence intervals and statistical significance are determined through bootstrap re-sampling. It yields accurate confidence intervals despite the data distribution and heteroscedasticity, and is also resistant to outliers.

The trends computed with *openair* were contrasted with those calculated using the MAKESENS 1.0 macro (Salmi et al., 2002) as follows. Firstly, the presence of a monotonic trend was tested with the non-parametric Mann-Kendal test. For the MCMA, GMA and MMA, the available yearly data are n>10, hence positive values in the Z parameter correspond to positive trends and vice-versa for negative values of Z. The significance of the estimated trend was tested at α=0.001, 0.01, 0.05 and 0.1 using a two-tailed test. Secondly, slopes of linear trends were calculated with the non-parametric Sen's method, which assumes linear trends, with a Q slope and a B intercept. To calculate Q, first the slopes of all data values were calculated in pairs, with the Sen's estimator slope as the median of all calculated slopes. Finally, 100(1-α) % two-sided confidence intervals about the slope estimate were obtained based on a normal distribution. Comparisons of estimated trends from both approaches are shown in the Supplementary information S1.4 (Fig. S4).

The O_3 and other air pollutant time-series were decomposed into trend, seasonal and residual components using the Seasonal-Trend Decomposition technique (STL; Cleveland et al., 1990). STL consists of two recursive procedures: an inner loop nested inside an outer loop, assuming measurements of x_i (independent) and y_i (dependent) for i = 1 to n. The seasonal and trend components are updated once in each pass through the inner loop; each complete run of the inner loop consists of $n_{(i)}$ such passes. Each pass of the outer loop consists of the inner loop followed by a computation of the robustness weights, which are used in the following run of the inner loop to minimise the influence of transient and aberrant behaviour on the trend and seasonal components. The initial pass of the outer loop is performed with all robustness weights equal to 1, followed by $n_{(0)}$ passes of the outer loop. The Kalman Smoother (KS) was used to provide minimum-variance, unbiased linear estimations of observations and to impute missing data to satisfy the STL (Reinsel, 1997; Durbin et al., 2012; Carslaw, 2015). Overall, statistical seasonal auto-regressive and moving averages with annual seasonal components were employed. Statistical analyses were carried out with SPSS 19.0.

In order to carry out seasonal analyses of data, seasons were defined according to temperature records in the NH, as described previously (Hernandez-Paniagua et al., 2015): winter (December-February), spring (March-May), summer (June-August) and autumn (September-November). Wind-sector analyses of data were performed by defining 8 wind sectors each of 45° starting from 0° ± 22.5°. The lower bound of each sector was established by adding 0.5° to avoid data duplicity. Data were assigned to a calm sector when wind speed was ≤ 0.36 km h^{-1} (0.1 m s^{-1}). To assess regional transport, air mass back-trajectories (AMBT) were calculated using the HYSPLIT model v.4 (NOAA Air Resources Laboratory (ARL); Stein et al., 2015), with the Global NOAA-NCEP/NCAR reanalysis data files on a latitude-

longitude grid of 2.5°, downloaded from the NOAA ARL website (http://ready.arl.noaa.gov/HYSPLIT.php). HYSPLIT frequency plots of 96-h AMBT were constructed for every 6 h during the year 2014 with an arrival altitude of 100 m above ground level.

3. Results

3.1 Wind occurrence at the MMA

The MMA is highly influenced by anti-cyclonic easterly air masses that arrive from the Gulf of Mexico, especially during spring and summer (Fig. S5). Figure 2 shows the frequency count of 1-h averages of wind direction by site and season within the MMA during 1993-2014. At all sites, apart from OBI, the predominant wind direction is clearly E, which occurs between 35-58 % of the time depending on season. Easterly air masses are augmented by emissions from the industrial area E of the MMA, which are transported across the urban core and prevented from dispersing by the mountains located S-SW of the MMA. On average, the highest wind speeds are observed during summer at all sites. By contrast, calm winds of ≤ 0.36 km h^{-1} (0.1 m s^{-1}) occurred less than 2 % of the time at all sites, most frequently in winter, and least frequently in summer.

3.2 Time-series in O_3 and O_X recorded within the MMA during 1993-2014

Within the MMA, the highest O_3 mixing ratios (1-h averages) are typically observed between April-September during the photochemical season, whereas the lowest values are usually recorded between December-January (winter) (Fig. S6). Table S1 summarises the minimum, maximum, average (mean) and median hourly O_3 mixing ratios recorded during 1993-2014. The highest O_3 mixing ratios recorded were 186 ppb at GPE in 1997, 146 ppb at SNN in 2004, and 224 ppb at SNB in 2001. At OBI and STA, the highest O_3 mixing ratios were both recorded on June 2, 1993: 182 ppb at 12:00 CDT at OBI, and 183 ppb at 13:00 CDT at STA, during the occurrence of E winds. Note that all times below are given in CDT. Annual O_3 averages varied from 14 ± 14 ppb at OBI in 2001 to 32 ± 23 ppb at SNB in 1993, whereas O_3 annual medians ranged from 10 ppb at OBI in 2001 to 28 ppb at SNN in 1993.

Reaction with O_3 rapidly converts NO to NO_2, and therefore mixing ratios of odd oxygen ($O_X = O_3 + NO_2$) were calculated to account for O_3 stored as NO_2 for each hour during 1993-2014 at the 5 sites within the MMA (Table S2; Fig. S7). Minimum values of O_X ranged from 2 ppb, observed at all sites mostly during 1993-2014 to 13 ppb at OBI in 2007. Maximum values of O_X ranged from 99 ppb at SNN in 2002, to 330 at OBI in 1993. O_X annual averages varied from 23 ± 17 ppb at SNN in 2002 to 51 ± 27 ppb at OBI and at STA in 2001 and 2006, respectively, whereas O_X annual medians ranged from 21 ppb at SNB and SNN, in 2001 and 2002, respectively, to 46 ppb at OBI and STA in 2001 and 2006, respectively. It is clear that the highest O_3 and O_X mixing ratios were recorded when control of precursor emissions of VOCs and NOx were less stringent than subsequently.

3.2 Diurnal variations in O_3 and O_X within the MMA

Diurnal variations in O_3 arise from the balance between its net production and destruction. Here, O_3 diurnal variations were used to assess changes in the net O_3 production. Figure 3 shows daily profiles by season of O_3, O_X, NO, NO_2, NO_X, and SR averaged over the 5 sites within the MMA. O_3 generally dips during the morning rush hour due to titration with NO and mirrors the increase in NO_2, which occurs around 07:00 in spring and summer, and around 08:00 in autumn and winter. The 1-h difference in the O_3 dip derives from the change to daylight saving time during spring and summer. O_3 generally peaks during the enhanced photochemical period, around 13:00 in spring, 12:00 in summer (co-incident with SR), and about 14:00 in autumn and winter. Similar profiles are observed for O_3 in all seasons, being negatively correlated with NO_2 (r=0.93 (winter) to r=0.97 (summer) (p<0.05)), due to the rapid photolysis of NO_2. Diurnal cycles of O_X behave as O_3, with lowest values before the morning rush hour and the largest between midday (summer) and 15:00 (winter). During daytime, O_X and O_3 diurnal cycles are strongly correlated in all seasons, ranging from r=0.97 in winter to r=0.99 in autumn (p<0.05), which suggests net O_3 production during daytime.

O_3 and O_X levels depend strongly on the photochemical processing of NO_X and VOCs emissions. To assess differences in the net O_3 production from site-to-site within the MMA, O_3 and O_X amplitude values (AV_d) derived from normalised daily cycles were used as proxy. The normalised daily cycles were constructed by subtracting daily averages from hourly averages. Figure 4 shows normalised O_3 daily cycles and Fig. S8 normalised O_X daily cycles. The lowest AV_ds both in O_X and O_3 occur in winter consistent with reduced SR and low photolysis rates, while the largest ones are seen in summer. It is clear that during the whole year, the largest AV_ds are recorded at sites downwind of the industrial emission sources, in particular at STA, while the lowest AV_ds are observed at upwind sites. The larger AV_ds at downwind sites indicate higher net O_3 production, derived from photochemical processing of air masses from the E sector. The AV_ds seen at upwind sites indicate that these are less affected by emissions from the largest part of the MMA and from the industrial area.

3.3. Annual cycles of O_3 and O_x within the MMA

Annual variations in O_3 and O_x are correlated positively with the seasonality of temperature, RH and SR (Camalier et al., 2007; Zheng et al., 2007). Annual averages cycle for those meteorological variables, O_3 and O_X were constructed by averaging monthly averages for the same month during the studied period. Figure 5a shows that O_3 exhibits the maxima during spring and minima in winter, with a downward peak in early autumn, behaviour characteristic of tropospheric O_3 in the NH. O_X peaks in spring and dips in summer, although it is evident that NO_X emissions lead to apparently similar O_X levels in winter and spring despite the decrease in O_3 levels. A correlation analysis among monthly averages for both O_3 and O_X with temperature, rainfall, RH and SR, revealed that the strongest relationship was between O_3 and SR (r= 0.72, p<0.001; Fig. 5a), with relationship evident with O_X.

Seasonal amplitude values (AV_s) provide insight into inter-annual variations in the net O_3 production in response to changes in precursor emissions and meteorology. The seasonal cycles in O_3 during 1993-2014 were determined by filtering monthly averages with the STL technique (Cleveland et al., 1990) (Fig. S9). O_3 AV_ss were calculated as the difference peak-to-trough (spring peak). An average O_3 AV_s of 15.1 ± 2.97 (1σ) ppb was calculated from 1993 to 2014 within the MMA, with the lowest O_3 AV_s of 10.3 ppb determined in 1998, and the largest O_3 AV_s of 19.0 ppb observed in 2014. Figure 5b shows that O_3 AV_s decreased significantly at all sites between 1993 and 1997-1998, at rates from 0.78 ppb O_3 yr^{-1} at GPE to 2.28 ppb O_3 yr^{-1} at SNN (Fig. 5c). O_3 AV_ss increased constantly (p<0.05) at all sites since 1998, ranging from 0.90 ppb O_3 yr^{-1} at GPE to 0.75 ppb O_3 yr^{-1} at SNN. O_X AV_ss exhibited no discernible trends at all sites for the whole studied period, although, SNN show a significant (p<0.05) decline during 1993-2001 (1.5 ppb yr^{-1}) and at STA show an increase during 2004-2010 (1.3 ppb yr^{-1}). The trends in O_X follow those observed for NO_X at SNN and STA during 1993-2014, which indicates that nearby industrial emissions have a significant contribution on the observed O_X levels within the MMA.

3.4. Long-term trends in O_3 and O_X within the MMA during 1993-2014

Quantifying the absolute changes in ground-level O_3 in response to trends in its precursor emissions is crucial to evaluate the impacts of air quality control (Parrish et al., 2009; Simon et al., 2015). The growing economy within the MMA has increased O_3 precursor emissions from point and area sources, due to the limited emissions control programs (INEGI, 2015; SDS, 2015). Moreover, predominant E-SE winds throughout the year transports primary pollutants and their oxidised products downwind from the industrial area, which can offset reductions in emissions from other sources. Here, to characterise changes in net O_3 production during 1993-2014 within the MMA in response to changes in its precursor emissions, long-term trends for daytime (06:00-18:00 CDT) O_3 and O_x measurements were derived by averaging data in seasonal periods. Seasonal averaging was used to minimise variability inherent in longer-term averages and the de-seasonalisation process avoids confounding overall trends, especially when seasons exhibit opposite trends. (Parrish et al., 2009).

Figure 6 shows seasonal trends in O_3 within the MMA, and Table 3 summarises the parameterisation of the trends. Significant increases (p<0.1) in O_3 are observed at all sites, apart from STA, in spring and summer, while in autumn, O_3 increases significantly only at SNN and SNB. The increases in O_3 range from 0.26 ppb yr^{-1} in spring at OBI to 0.47 ppb yr^{-1} in summer at SNN. Overall, the lowest O_3 growth rates are observed at the urban background GPE site, whereas the largest ones are at the industrial SNN site. It is worth nothing that only SNN and OBI exhibit significant increases in autumn, despite a decrease in the frequency of high wind speeds (>20 km h^{-1}). The existence of significant trends at all sites during spring-summer, except for OBI, is consistent with the downwind transport of industrial emissions and the high frequency of photochemical processed air masses with NE-S-SE origin, where the industrial area is located (Fig. S10).

Seasonal trends in O_X are shown in Fig. 7, with the parameters of the trends listed in Table 3. Consistent with the seasonal O_3 trends observed, significant increases (p<0.1) in O_X within the MMA are determined in spring at all sites except for STA, and range from 0.02 ppb yr^{-1} at OBI to 0.67 ppb yr^{-1} at SNB. It is worth nothing that the industrial SNN and SNB sites show significant increases in O_X in all seasons, with the lowest growth rates in winter and the largest in summer and spring, respectively. Moreover, STA exhibits the only significant decrease in O_X of 0.63 ppb yr^{-1} during winter. As for O_3, the O_X increasing trends are consistent with the transport of primary emissions during the high occurrence of NE-E-SE air masses at WS >10 km h^{-1}, which is highlighted during the photochemical season (April-September). Furthermore, the small shift in wind direction at STA to NW during winter coincides with the only observed decrease in net O_3 production within the MMA, which confirms that O_3 precursors are emitted E of the MMA. This also makes evident that increasing upwind industrial emissions have offset reductions in emissions from on-road sources as revealed by the decline in NO_X evident at OBI.

3.5 Comparison of MMA O_3 and O_X weekly profiles with those at MCMA and GMA

O_3 production varies from city-to-city in response to local NO_x and VOCs emissions. Assessment of weekly profiles of O_3 and O_X may provide insights of the geographic response in net O_3 production to diurnal variations in precursor emissions. Hourly O_3 and O_X averages were used to construct weekday and weekend average profiles for the MCMA from 1993 to 2014, and for the GMA from 1996 to 2014. Figure 8 compares weekly O_3 and O_x profiles by season within the MMA with those for the MCMA and GMA. In each case, and consistent with observations in other major urban areas of NA, the lowest O_3 mixing ratios occur during the morning rush hour due to O_3 tritation with NO emitted from on-road sources, whereas peak values of O_3 are apparent after mid-day during periods of enhanced SR (Stephens et al., 2008; Jaimes-Palomera et al., 2016). It should be noted that the peak value of O_3 for the GMA in winter and spring occurs an hour or so earlier than for the MMA and MCMA, which is consistent with higher VOC/NO_x emissions ratios at the GMA (Kanda et al., 2016). As might be anticipated, larger AV_d of 76.9 ± 1.6 ppb O_3 are observed for the MCMA than for the GMA (46.1 ± 1.0 ppb O_3) and MMA (37.6 ± 0.4 ppb O_3), related to the levels of emissions of the O_3 precursors. The O_X profiles show a trough during the morning rush hour and a peak between 12:00 and 14:00 at all urban areas. Despite large variations between weekday and weekend NO_X mixing ratios at the 3 urban areas as shown in Fig. 8, no significant differences (p>0.05) in O_3 and O_X are observed at any of the metropolitan areas between O_3 and O_x weekends and weekdays AV_ds.

Stephens et al. (2008) suggested that the most plausible explanation for the lack of weekend O_3 effect at MCMA during 1987-2007, is that weekday O_3 production is limited by VOCs and inhibited by NO_X. Therefore, the very similar levels O_3 observed during weekdays and weekends can be explained by simultaneous decreases in NO_X and VOCs emissions and the resulting effects on net O_3 production. Similarly, a VOC-limited O_3 production regime was reported for the MMA by Sierra et al. (2013), whereas Kanda et al. (2016) reported that at the GMA the O_3 production lies in the region between VOC- and

NO_X-sensitivity. Therefore, it can be hypothesised that simultaneous decreases in emissions of NO_X and VOCs during weekends at the GMA and MMA explain the similarity in behaviour in O_3 and O_X as at the MCMA. Indeed, Wolff et al. (2013) reported that at several urban areas of the US, similar or even higher (±5 %) O_3 levels during weekdays than at weekends were due to lower O_3 precursor emissions over weekends. Furthermore, the number of sites in the US that exhibited a weekend effect decreased from ca. 35 % to less than 5 % from 1997-1999 to 2008-2010, which was attributed to an increase in the VOC/NO_X emission ratio derived from a greater decline in NO_X than in VOCs emissions, mostly driven by reductions from on-road sources. A change to a NO_X-limited O_3 production regime during weekends at the three urban areas seems unlikely, since this would result in lower O_3 levels during weekends, which is not observed at any of the studied urban areas (Torres-Jardon et al., 2009).

3.6 Long-term trends at MCMA, GMA and MMA from 1993 to 2014

The high mixing ratios of O_3 observed typically at the 3 largest urban areas in Mexico have motivated the introduction of control strategies to decrease emissions of the O_3 precursors, NOx and VOCs. The success of the control strategies implemented can be evaluated by assessing trends in O_3 and O_X. As for the MMA, seasonal trends in O_3 and O_X within the MCMA and GMA were calculated from daytime measurements. Figure 9 shows a comparison of inter-annual trends in O_3 and O_X at the 3 urban areas in Mexico, and Table 4 lists the parameters of the trends. Overall, during 1993-2014, daytime O_3 at the MCMA decreased significantly (p<0.05) by 1.15 ppb yr^{-1} (2.04 % yr^{-1}), and increased at the MMA by 0.22 ppb yr^{-1} (0.84 % yr^{-1}); at the GMA no discernible trend was observed during 1996-2014. For daytime O_X at the MCMA and GMA during the same periods, significant decreases (p<0.05) of 1.87 and 1.46 ppb yr^{-1} were determined, respectively, while the MMA does not exhibit a significant change. At the MCMA, the overall trends in O_3 and O_X are strongly driven by their wintertime decreases of 1.62 and 2.47 ppb yr^{-1}, respectively; whereas at the MMA, the annual growth in O_3 is driven by increases in spring and summer of 0.32 and 0.27 ppb yr^{-1}, respectively. Although, at the MMA, an increase in O_X of 0.28 ppb yr^{-1} is observed only during summer, the overall O_X trend is strongly affected by the non-significant trends in the other seasons. It is worth nothing that at the GMA, the overall decrease in O_X of 1.46 ppb yr^{-1} is similar for all seasons, which range between 1.40 ppb yr^{-1} (autumn) and 1.89 ppb yr^{-1} (spring).

The overall trends in net O_3 production during 1993-2014 at the MCMA and GMA are consistent with the significant (p<0.05) annual decreases in NO_X of 1.21 and 1.25 ppb yr^{-1}, respectively (Fig. 10). By contrast, while average NO_X levels have increased annually at the MMA at 0.33 ppb yr^{-1} (p<0.05), the average net O_3 production has remain steady. Either the non-linear response in O_X to the changes in NO_X in an environment of high NO_X mixing ratios (>60 ppb) displace the chemical equilibrium to favour NO as the dominant component of NO_X which does not account for the levels of O_X (Clapp and Jenkin, 2001). Or the O_X trends derived from the combined data set for the MMA do not represent local observed trends, because a compensating effect between O_X reductions and increases.

3.7 Compliance with the 1-h and 8-h Mexican Standards for O_3 within the MMA

Between 1993 and 2014, there were two official standards for maximum permitted mixing ratios of O_3 in Mexico: i) a running 8-h average of 80 ppb, not to be exceeded more than 4 times per calendar year, and ii) a 1-h average of 110 ppb (NOM-020-SSA1-1993). Since 19 Oct 2014, the maximum permitted O_3 levels were lowered to a running 8-h average of 70 ppb and a 1-h average of 95 ppb, (NOM-020-SSA1-2014). However, because both standards are applicable for whole calendar years, the old permitted O_3 levels were used in this study to determine the number of annual exceedances to both O_3 standards. Figure 11 shows that within the MMA, the O_3 1-h average and the running 8-h standards were frequently exceeded (INE, 2011; SEMARNAT, 2015). The largest number of exceedances occurs at STA, followed by SNB, GPE and OBI, whereas the fewest breaches are observed at SNN markedly since 2004. However, there have been 3 periods of clear decreased exceedances at all sites (except STA in 2014), during 1994-1995, 1999-2000, and 2012-2013, which are consistent with marked changes in the national GDP during economic recessions in Mexico (Fig. S11a). However, although, national GDP exhibits a notable decrease during the 2008-2009 global economic recession, only in 2009 do the O_3 annual exceedances within the MMA seem to follow (Fig. S11b).

Therefore, if O_3 levels continue to increase within the MMA, as determined in the long-term trend assessment, an increase also in peak O_3 mixing ratios is likely to occur. Hence, to analyse changes in peak O_3, daily maxima 1-h averages from 1993 to 2014 were used to determine seasonal trends in peak levels. Figure 12 shows trends in 1-h daily maxima and Table 5 list the parameters of the trends. Daily maxima O_3 1-h averages have increased significantly (p<0.05) in spring and summer at all sites, except for STA, and also in autumn at the industrial sites SNN and SNB. The largest increases in the daily maxima are seen at SNN, where similar increases between 0.85 and 0.93 ppb yr^{-1} are determined between spring and autumn. SNB exhibits slightly lower growth rates in spring and summer, but a large difference in autumn. We have shown that predominantly E-SE winds transport photochemically processed air mases to SNN and SNB during spring-summer leading to the observed exceedances. Moreover, the change in the wind occurrence in autumn at SNB leads to a lower growth rate than at SNN, where the calmest winds during the whole year drive the largest increase interpreted to be due to the photochemical processing of precursors emitted locally. The GPE and OBI sites exhibit increases only in spring and summer, with the lowest increases of all sites determined at OBI of 0.48 ppb yr^{-1} in spring, which contrasts with the largest increase at OBI during the same season. However, such increases are consistent with an increase in the occurrence of NE and E air masses at high speeds (>10 km h^{-1}) during spring-summer. STA shows a significant decrease in the maxima daily O_3 1-h averages of 0.35 ppb yr^{-1} in winter, which is consistent with an increase in the occurrence of NW air masses at WS < 5 km h^{-1}, loaded with high NO_x mixing ratios (50 ppb) that promote the O_3 titration.

4. Discussion

4.1 Strategies for air quality control in Mexico

The Mexican environmental authorities have focused largely on improving the air quality within the MCMA since 1986, by implementing numerous strategies to control primary emissions, but have paid less attention to other large metropolitan areas in Mexico (PICCA, 1990; ProAire-MCMA, 2011). Control measures have been designed based on NAEI and local emission inventories data, which possess significant uncertainties (Arriaga-Colina et al., 2004; Velasco et al., 2007; Kanda et al., 2016). However, despite these uncertainties, the emission control strategies have helped to reduce O_3 levels within the MCMA since 1991-1992 (ProAire-MCMA, 2001). Here, we describe the most effective measures introduced to control O_3 precursor emissions within the MCMA, and then discuss potential benefits of implementing such measures within the MMA.

From 1993 to 2014, NO_X levels within the MCMA decreased at a rate of around 1.2 ppb yr^{-1} (1.6 % yr^{-1}) as determined from ground-based measurements. This decline is remarkably consistent with the decrease during 2005-2014 in the NO_2 column over the MCMA of 1.6 % yr^{-1} reported by Duncan et al. (2016). The decrease in NO_X has been driven largely by reductions in emissions from on-road sources, in response to the introduction of mandatory 3-way catalytic converters in new vehicles since 1993 (NOM-042; SEMARNAT, 1993), and by the introduction of a no driving day and more stringent exhaust emissions inspection programs for private cars since 1989 (NOM-041; SEMARNAT, 1993). The NO_X reduction measures also required public transport vehicles to switch from petrol to LP gas fuelled engines, new road corridors were designed for improving the intracity transport and the public transport fleet was renewed (ProAire-MCMA, 2001). For industrial sources, the switch from fuel oil to LP gas fuel, relocation of highly polluting industries away from the MCMA, and implementation of regular inspections programs of NO_X emission for industrial and area sources were also implemented (ProAire-MCMA, 2001).

While the outlook for NO_X levels within the MCMA is clear, studies of VOCs levels have reported no concluding trends. For instance, Arriaga-Colina et al. (2004) reported a decrease in VOCs of around 10 % from 1992 to 2001 over the N MCMA, while Garzón et al. (2015) reported that on average VOCs increased over most of the MCMA between 1992-2002 but decreased by 2.4 ppb yr^{-1} between 2002-2012. However, the decrease in VOCs from 2002 to 2012 reported by Garzón et al. (2015) is consistent with a reduction in light alkanes and aromatics levels during the morning rush hour reported by Jaimes-Palomera et al. (2016). Continuous measurements of VOCs have been introduced recently by the MCMA government, which precludes an assessment of VOCs long-term trends. The measures implemented to control VOCs emissions from on-road sources have included the reformulation of petrol with the reduction of highly reactive VOCs and addition of oxygenated compounds, and fitting of 3-way catalytic converter in all new vehicles (NOM-042; SEMARNAT, 1993; ProAire-MCMA, 2001). For area sources, control measures include the introduction of vapour emissions control systems at petrol stations and introduction of a LP gas leak detection program for the distribution network (ProAire-MCMA, 2011). As

for NO_X, industrial VOCs emission sources have been subject to regular emissions inspections and relocation of the most significant emitters (ProAire-MCMA, 2011).

Therefore, the moderate success on controlling O_3 levels within the MMA can be interpreted as the implementation of effective controls measures on VOCs and NO_X emissions. Thus, a comparison between VOCs and NO_X trends derived from the NAEI and local emissions inventories with those determined from ground-levels measurements can provide insight into further improvements in decreasing O_3 levels not only within the MCMA but also at other large metropolitan areas in Mexico. Within the MCMA, the NAEI NO_X emissions trends are consistent with the decrease determined from ground-based measurements made by SIMAT, but the MCMA local inventory trends disagree with the SIMAT trends (Fig. S1 and Fig. 10). For VOCs, the NAEI and the MCMA inventories oppose measured trends in VOCs during 1993-2001 (Arriaga-Colina et al., 2004; Garzón et al., 2015). This can be explained by underestimates of VOC emissions within the MCMA of a factor of 2-3 (Arriaga-Colina et al., 2004; Velasco et al., 2007). Such discrepancies suggest that, significant improvements in NO_X and VOCs emissions inventories are still required to better inform O_3 control strategies.

4.2 Ground-level O_3 and O_X variations within the MMA

The O_3 and O_x diurnal variations result from the particular chemical environment and meteorological conditions at each monitoring site within the MMA. Thus, the largest O_3 and O_X mixing ratios, except for OBI, are observed typically for air masses from the E and SE wind sectors, whereas at OBI, the largest O_3 and O_X values are recorded during the occurrence of NE and E air masses. It is clear that short-range transport and large upwind emissions of O_3 precursors from the industrial area dominate the MMA (SEMARNAT, 2006, 2011, 2014; SDS, 2015). This is underlined at OBI with the highest values of O_X where the predominant wind direction is NE, consistent with the transport of emissions from the industrial area located NE, and photochemical processing of air masses (Carrillo et al., 2017). The daily cycles of O_3 determined within the MMA are consistent with those reported for Los Angeles (VanCuren, 2015), and Toronto (Pugliese et al., 2014). At Toronto, the O_3 maxima were enhanced by the arrival of photochemical processed air masses transported from polluted wind sectors, and decreased during clear air masses. This behaviour is similar to that observed within the MCMA with enhanced O_3 maxima during the occurrence of E-SE (polluted) and decreased levels when SW-W (relatively clean) air masses occurred.

4.3. Origin of the O_3 annual cycles within the MMA

The O_3 annual cycles within the MCMA are consistent with the spring maxima and winter minima characteristic of the US southeast regions (Strode et al., 2015), and follow the O_3 cyclic pattern at NH mid-latitudes (Monks 2000; Vingarzan, 2004). However, they are different to O_3 annual cycles reported for the US west coast regions, particularly in California, where the maxima in the cycle occurs between June-August, driven the local influence of precursor emissions upon O_3 production and photochemical

conditions (Vingarzan, 2004; Strode et al., 2015). The recurrent downward spikes in the O_3 annual cycles within the MMA between July-August result from high wind speeds (>10 km h^{-1} on average) that disperse O_3 precursors and increase the boundary layer height (ProAire-MMA, 2008). The peak in O_3 observed in September is characteristic of humid regions, and can be ascribed to an increase in OH radicals derived from the increment in RH during the rainy season (Lee et al., 2014). A marked increase in RH within the MMA during September is consistent with the increase in O_3 observed as reported by Lee et al. (2014). Over the mid-western and eastern US regions, that O_3 peak has become less noticeable since 2000 (Zheng et al., 2007).

The annual variability in O_3 within the MMA is strongly coupled to the economic conditions (GDP) in Mexico. For instance, the economic crisis of 1994-1996 caused a marked reduction in industrial emissions of VOCs and NO_X, which is confirmed by the significantly decrease in O_3 annual variations at all sites within the MMA (Tiwari et al., 2014; INEGI, 2016). During the global economic recession of 2008-2009, Castellanos and Boersma (2012) reported a reduction of 10-30 % in tropospheric NO_2 over large European urban areas, which is consistent with a faster decline of 8 ± 5 % yr^{-1} in the NO_2 column density during the same period for US urban regions (Russell et al., 2012). Increases in the NO_2 column density over the MMA as reported by Duncan et al. (2016) are explained by the gradual recovery of the economy since 1997 in Mexico. Moreover, increases in O_3 precursor emissions and in annual variability observed within the MMA are consistent with such economic growth. This explains clearly the opposite trends in O_3 annual variations before and after the economic crisis within the MMA, with the lowest changes seen at the urban GPE site and the greatest ones detected for the SNN industrial site.

4.4 Increasing O_3 and O_X levels within the MMA

Ground-based measurements made during 1993-2014 reveal significant (p<0.05) increases in NO_X within the MMA at all sites, apart from OBI, which exhibits a significant decrease (Fig. 13). Overall, the NO_X increase within the MMA of 1.24 % yr^{-1} (0.33 ppb yr^{-1}) during 1993-2014 is larger than the increase in the NO_2 column density over the MMA of around 0.78 % yr^{-1} during 2005-2014 reported by Duncan et al. (2016), although both indicate a significant increase in the NO_X levels at least since 2005. The largest increases in NO_X correspond to industrial sites, SNN (0.51 ppb yr^{-1}) and SNB (0.74 ppb yr^{-1}), which is interpreted as a response to growing industrial activity, in combination with flexible emission regulations within the MMA (INEGI, 2016). The influence of industrial emissions upon O_3 at the MMA becomes evident by the lowest NO_X growth rate observed at GPE of 0.19 ppb yr^{-1}, since OBI has few occurrences of air masses transporting pollutants from the largely industrialised areas throughout the year (Fig. 2). By contrast, the NO_X decrease at OBI of -0.40 ppb yr^{-1} arises from decreases in emissions from on-road sources (SDS, 2015). The large growth rates in O_3 and NO_X at SNN and SNB are explained by increasing emissions of O_3 precursors from a growing number of industries and the urban development E of the MMA. The most likely explanation for the O_3 increase at OBI is a reduced titration effect by decreasing

607 NO_X levels in combination with the non-linear response in O_3 production to decreasing NO_X emissions
608 under the VOC-sensitive MMA airshed (Sierra et al., 2013; Menchaca-Torre et al. 2015).
609
610 The O_3 increasing trends within the MMA are opposite to those reported by Sather and Cavender (2016)
611 at 4 South Central US urban areas, where NO_X and VOCs decreased by 31-70 % and 43-72 % during
612 1983-2015, respectively, resulting in a reduction between 18-37 ppb O_3 in the 8-h averages. The O_3
613 response to NO_X decreases at OBI is similar to that observed in central London during 1996-2008 (Bigi
614 and Harrison, (2010), and at four urban areas in Japan during 1990-2010, explained by the decrease of
615 the NO titration effect (Akimoto et al., 2015). This suggests that controlling VOCs emissions may lead to
616 a decrease in the net O_3 production, whereas decreases in NO_X may not have significant effects on O_3
617 production or even increase the O_3 levels due existence of a VOC-limited environment within the MMA
618 (Sierra et al., 2013, Carrillo et al., 2017).
619
620 The O_X long-term trends during 1993-2014 within the MMA were consistent with those for O_3 at all sites.
621 Decreases in NO_X and O_3 observed between 1994-1996 were the response to the economic crisis during
622 the same period in Mexico, when the DGP decreased by 5.9 % providing additional evidence of the
623 dominant role of industries within the MMA. Consistent with economic indicators, annual averaged petrol
624 sales in the Nuevo Leon state in 1995 decreased by 2.4 % in relation to 1994, but increased linearly from
625 1996 to 2008 at an approximate rate of 98,800 m^3 petrol yr^{-1} ($r = 0.90$) (Fig. S12) (SENER, 2015). As for
626 petrol sales, registered vehicles in Nuevo Leon show significant variations between 1993-1996, but
627 increase linearly since 1997 at a rate of around 100,000 vehicles yr^{-1} ($r=0.99$). This confirms that despite
628 the annual growth in the vehicular fleet, the fitting of 3-way catalyst technology and reformulation of petrol
629 introduced in 1997 has controlled on-road primary emissions (ProAire-MCMA, 2001) The decreases in
630 NO_X observed at OBI and at all sites during the occurrence of SW-W-NW air masses reflect that if
631 applied, stricter emissions controls such as those for on-road sources can lead to a significant abatement
632 in primary emissions. It is clear that the industrial sources must be subject to similar emission control
633 measures as those implemented within the MMA for effectively reducing the O_3 levels.
634
635 **4.5 The opposite O_3 trends at Mexican urban areas**
636 The comparison of O_3 and O_X trends at MMA, GMA and MCMA reveals different emission trends at each
637 of the studied cities. The trends in O_3 reported in this study for the MCMA, agree with the reduction of
638 20 ppb O_3 during 1991-2011 for the MCMA (Jaimes et al., 2012), and with the reduction of 8 ppb O_3
639 during 2000-2011 for the MMA (Benítez-García et al., 2014). At the GMA, the no trend status in O_3
640 determined here is in contrast with the increase of 12 ppb O_3 during 2000-2011 (Benítez-García et al.,
641 2014), which is due to the different periods assessed in the latter. Decreases in O_3 in US urban areas
642 arise from effective control of O_3 precursor emissions (Strode et al., 2015), which has occurred at the
643 MCMA. By contrast, O_3 levels increased in urban areas of Japan by 0.22-0.37 ppb yr^{-1} (Akimoto et al.,
644 2015), and in the Greater London by 0.5 ppb yr^{-1} (Bigi and Harrison, 2010), due to faster declines in NO_X

than in VOCs and are slightly similar that observed in O_3 averages for the MMA (0.20 ppb yr^{-1}), where average NO_X levels have increased and also likely VOCs.

Trends in net O_3 production can be interpreted as the response to trends in its precursors, which also respond to implemented policies to control their emissions and to economic factors. Figure 10 shows that NO_X decreased significantly within the MCMA (1.57 % yr^{-1}) and the GMA (1.83 % yr^{-1}) during 1993-2014 and 1996-2014, respectively, but increased within the MMA (1.83 % yr^{-1}) during 1993-2014. Such NO_X trends are within the range of the trends in the NO_2 column density reported by Duncan et al. (2016) in Table S9, which reveals an increase of 0.78 ± 1.12 % yr^{-1} for the MMA, but decreases of 1.82 ± 0.84 % yr^{-1} for the GMA and of 0.10 ± 1.67 % yr^{-1} for the MCMA, all during 2005-2014. To date, long-term trends in VOCs have only been reported only the MCMA with an average decrease of ca. 2.4 ppb yr^{-1} since 2002, mostly in propane, ethanol and acetone (Garzón et al., 2016), while there are no studies of long-term trends in VOCs within the MMA and the GMA.

It is clear that O_3 and O_X decreases within the MCMA have been driven by reductions in NO_X and VOCs emissions, and that the implemented strategies described in Sect. 4.1 have proved to be effective in controlling primary emissions. By contrast, growing industrial emissions within the MMA must be subject to stringent controls to abate O_3 levels. In the GMA, where the industrial activity is lower that at the MCMA and MMA (Kanda et al., 2016), the policies introduced at national scale for controlling on-road sources emissions have resulted in the decrease of NO_X emissions and in the stabilisation of O_3 levels. Finally, the results presented here demonstrate the merits of the assessment and analysis of long-term O_3 levels, which can be used by environmental authorities to revise and to redesign programs and policies to improve air quality. Continuing with ground-based O_3 and NO_X monitoring is strongly recommended to better understand the response further changes in local and regional O_3 levels to changes in primary emissions. Monitoring of VOCs at the GMA and MMA is also recommended to as the VOCs emissions data reported in the NAEI possess significant uncertainties.

5. Conclusions

Diurnal and annual cycles, and long-term trends in O_3 and O_X within the MMA, are interpreted as response to changes in NO_X and VOCs emissions, photochemistry and meteorology. Continuous high-frequency and high-precision O_3 and NO_X data recorded during 1993-2014 at 5 sites within the MMA and at 29 sites within the MCMA, and during 1996-2014 at 10 sites within the GMA, were used to calculate long-term trends. Within the MMA, the greatest mixing ratios in O_3 were recorded during E and SE winds, at sites downwind of significant precursors from industrial sources. By contrast, the lowest O_3 mixing ratios were recorded at SNN, and for all sites were observed for the W and SW sectors, where air masses travel from central Mexico over 100-300 km of semi-arid region sparsely populated. Maximum daily 1-h values of O_3 and O_X increased significantly at GPE, SNN and SNB, owing to increasing

emissions of precursors, while at OBI increasing O_3 and decreasing O_X trends arise from the non-linear response to decreasing NO_X emissions from on-road sources.

Annual cycles in O_3 at all sites peak in spring and through in winter, with a downward spike during summer caused by high winds that disperse O_3, and increase the boundary layer height. Decreases in O_3 precursor emissions during the economic crisis experienced in Mexico between 1994-1996, caused significant decline trends O_3 annual variations from 1993 to 1997 or 1998, depending on site, followed by significant increases derived from the recovery of the economy. The dominant role of industrial sources on O_3 precursor levels within the MMA was evident at the industrial site SNN during the 1994-1996 economic crisis.

At all metropolitan areas studied, O_3 and O_X levels showed no significant differences between weekdays and weekend, although an earlier occurrence of the O_3 peak at the GMA was detected, ascribed to larger VOCs/NO_X emission ratio. The lack of the weekend effect was attributed to weekday O_3 production being limited by VOCs, whereas increases in the VOC/NO_x ratio during weekends in response to reduced emissions from mobile sources resulted in similar O_3 mixing ratios that during weekdays. Larger AV_ds during weekdays and weekends were seen at MCMA than at GMA and MMA related to the relative emissions of the O_3 precursors.

Significant seasonal trends in O_3 and O_X during spring were observed at all sites, apart from STA, whereas industrial sites exhibited significant increases for O_X in all seasons. The largest increases in O_3 and O_X were observed during the occurrence of NE-E-SE air masses. The only significant decrease in O_X at STA was related to the NW wind occurrence during winter. NO_X mixing ratios increased significantly at all sites, except at OBI, due to the dominant role of industrial sources on NO_X levels. The overall significant increasing trend of 0.22 ppb O_3 yr^{-1} within the MMA contrasts within a significant decreasing trend of 1.15 ppb O_3 yr^{-1} within the MCMA during 1993-2014, whereas a non-significant trend is evident within the GMA during 1996-2014. At the MCMA and GMA, the overall O_X trends reflect the trends in O_3 precursors. According to the long-term trends in O_3 for the MMA, the number of exceedances of the air quality standards will very likely increase as result of increasing precursor emissions. The moderate mitigation of O_3 levels within the MCMA, derived from measures implemented to controle missions from on-road, industrial and area sources, emphasises the need for more stringent control of emissions mostly from industrial sources within the MMA in order to improve air quality. Finally, comparison between emission inventories estimates of NOx and VOCs with ground-based measurements, indicate that significant reductions in uncertainties are required to better inform air quality policies.

6. Acknowledgments

This research was supported by Tecnologico de Monterrey through the Research Group for Energy and Climate Change (Grant 0824A0104 and 002EICIR01). Grateful acknowledgements are made to the

Secretariat for Sustainable Development of the Nuevo Leon State, the Secretariat for the Environment of Mexico City and the Secretariat for the Environment and Territorial Development of the Jalisco State for the public domain records. We gratefully thank the NOAA Air Resources Laboratory (ARL) for access to the HYSPLIT model and READY website (http://www.ready.noaa.gov), and Dr. Sigfrido Iglesias for providing the imputed O_3 and NO_x data for the MMA time-series. We are also grateful to Professor Paul Monks and Professor Richard Derwent for encouraging comments on an earlier version of the manuscript.

7. References

Akimoto, H., Mori, Y., Sasaki, K., Nakanishi, H., Ohizumi, T., and Itano, Y.: Analysis of monitoring data of ground-level ozone in Japan for long-term trend during 1990-2010: Causes of temporal and spatial variation, Atmos. Environ., 102, 302-310, doi:10.1016/j.atmosenv.2014.12.001, 2015.

Arriaga-Colina, J. L., West, J. J., Sosa, G., Escalona, S. S., Ordunez, R. M., and Cervantes, A. D. M. Measurements of VOCs in Mexico City (1992–2001) and evaluation of VOCs and CO in the emissions inventory, Atmos. Environ., 38, 2523-2533, doi:10.1016/j.atmosenv.2004.01.033, 2004.

Atkinson, R.: Atmospheric chemistry of VOCs and NOx. Atmos. Environ., 34, 2063-2101, doi:10.1016/S1352-2310(99)00460-4, 2000.

Benítez-García, S. E., Kanda, I., Wakamatsu, S., Okazaki, Y., and Kawano, M.: Analysis of criteria air pollutant trends in three Mexican metropolitan areas, Atmosphere, 5, 806-829, doi:10.3390/atmos5040806, 2014.

Bigi, A., and Harrison, R. M.: Analysis of the air pollution climate at a central urban background site, Atmos. Environ., 44, 2004-2012, doi:10.1016/j.atmosenv.2010.02.028, 2010.

Boersma, K. F., Jacob, D. J., Bucsela, E. J., Perring, A. E., Dirksen, R., van der A, R. J., Yantosca, R. M., Park, R. J., Wenig, M. O., Bertram, T. H., and Cohen, R. C.: Validation of OMI tropospheric NO_2 observations during INTEX-B and application to constrain NOx emissions over the eastern United States and Mexico, Atmos. Environ., 42, 4480-4497. doi:10.1016/j.atmosenv.2008.02.004, 2008.

Butler, T. M., Stock, Z. S., Russo, M. R., Denier Van Der Gon, H. A. C., and Lawrence, M. G.: Megacity ozone air quality under four alternative future scenarios, Atmos. Chem. Phys., 12, 4413-4428, doi:10.5194/acp-12-4413-2012, 2012

Camalier, L., Cox, W., and Dolwick, P.: The effects of meteorology on ozone in urban areas and their use in assessing ozone trends, Atmos. Environ., 41, 7127-7137, doi: 10.1016/j.atmosenv.2007.04.061, 2007.

Carrillo-Torres, E. R., Hernández-Paniagua, I. Y., and Mendoza, A.: Use of Combined Observational- and Model-Derived Photochemical Indicators to Assess the O_3-NO_x-VOC System Sensitivity in Urban Areas. Atmosphere, 8, 22, doi:10.3390/atmos8020022, 2017.

Carslaw, D. C., and Ropkins, K.: openair - An R package for air quality data analysis, Environ. Model. Soft., 27-28, 52-61, doi:10.1016/j.envsoft.2011.09.008, 2012.

Carslaw, D. C.: The openair manual - open-source tools for analysing air pollution data, Manual for version 1.1-4, King's College London, 2015.

Castellanos, P. and Boersma, K. F.: Reductions in nitrogen oxides over Europe driven by environmental policy and economic recession, Sci. Rep., 2, doi:10.1038/srep00265, 2012.

761 Clapp, L. J., and Jenkin, M. E.: Analysis of the relationship between ambient levels of O_3, NO_2 and NO
762 as a function of NO_x in the UK. Atmospheric Environment, 35, 6391-6405, doi: 10.1016/S1352-
763 2310(01)00378-8, 2001.

764 Cleveland, R. B., Cleveland, W. S., McRae, J., and Terpenning, I.: STL: A seasonal-trend decomposition
765 procedure based on Loess, J. Off. Stats., 6, 3-33, 1990.

766 Dentener, F., Stevenson, D., Cofala, J., Mechler, R., Amann, M., Bergamaschi, P., Raes, F., and
767 Derwent, R.: The impact of air pollutant and methane emission controls on tropospheric ozone and
768 radiative forcing: CTM calculations for the period 1990-2030, Atmos. Chem. Phys., 5, 1731-1755,
769 doi:10.5194/acp-5-1731-2005, 2005.

770 Duncan, B. N., Lamsal, L. N., Thompson, A. M., Yoshida, Y., Lu, Z., Streets, D. G., Hurwitz, M. M., and
771 Pickering, K. E.: A space-based, high-resolution view of notable changes in urban NO_x pollution around
772 the world (2005–2014), J. Geophys. Res., 121, 976–996, doi:10.1002/2015JD024121, 2016.

773 Durbin, J., and Koopman, S. J.: Time Series Analysis by State Space Methods, Oxford University Press,
774 Oxford UK, 2nd Edition, 2012.

775 EPA (Environmental Protection Agency US): Compilation of Air Pollution Emission Factors (AP-42),
776 Volume I: Stationary Point and Area Sources, available at: https://www.epa.gov/air-emissions-factors-
777 and-quantification/ap-42-compilation-air-emission-factors, last access: 14 Jan 2017, 1995.

778 EPA (Environmental Protection Agency US): User's Guide to MOBILE6.1 and MOBILE6.2: Mobile
779 Source Emission Factor Model, available at: https://www3.epa.gov/otaq/models/mobile6/
780 420r03010.pdf, last access: 16 Jan 2017, 2003.

781 EPA (Environmental Protection Agency US): Air quality trends, available at: https://www.epa.gov/air-
782 trends, last access: 15 Jan 2017, 2009.

783 Garzón, J. P., Huertas, J. I., Magaña, M., Huertas, M. E., Cárdenas, B., Watanabe, T., Maeda, T.,
784 Wakamatsu, S., and Blanco, S.: Volatile organic compounds in the atmosphere of Mexico City, Atmos.
785 Environ., 119, 415-429, doi:10.1016/j.atmosenv.2015.08.014, 2015.

786 Guicherit, R., and Roemer, M.: Tropospheric ozone trends, Chemosphere, 2, 167-183,
787 doi:10.1016/S1465-9972(00)00008-8, 2000.

788 Hernández-Paniagua, I. Y., Lowry, D., Clemitshaw, K. C., Fisher, R. E., France, J. L., Lanoisellé, M.,
789 Ramonet, M., and Nisbet, E. G.: Diurnal, seasonal, and annual trends in atmospheric CO_2 at southwest
790 London during 2000-2012: Wind sector analysis and comparison with Mace Head, Ireland, Atmos.
791 Environ., 105, 138-147, doi: 10.1016/j.atmosenv.2015.01.02, 2015.

792 INE (Instituto Nacional de Ecologia): Cuarto almanaque de datos y tendencias de la calidad del aire en
793 20 ciudades Mexicanas 2000-2009, INE-SEMARNAT, México, D.F., 405 pp., 2011.

794 INEGI (National Institute of Statistics and Geography): XIII Censo General de Población y Vivienda 2010,
795 México, available at: http://www.censo2010.org.mx/, last Access: 22 May 2016, 2010.

796 INEGI (National Institute of Statistics and Geography): México en Cifras, México, available at:
797 http://www3.inegi.org.mx/sistemas/mexicocifras/default.aspx?e=19, last access: 22 May 2016, 2015.

798 INEGI (National Institute of Statistics and Geography): Producto Interno Bruto (GDP)–Trimestral 2016,
799 available at: http://www.inegi.org.mx/est/contenidos/proyectos/cn/pibt/, last access: 11 Jan 2017, 2016.

800 IPCC: Climate Change 2013: The Physical Science Basis. Contribution of Working Group I to the Fifth
801 Assessment Report of the Intergovernmental Panel on Climate Change, 2013. [Stocker, T.F., D. Qin, G.-
802 K. Plattner, M. Tignor, S.K. Allen, J. Boschung, A. Nauels, Y. Xia, V. Bex and P.M. Midgley (eds.)].
803 Cambridge University Press, Cambridge, United Kingdom and New York, NY, USA, 1535 pp., 2013.

804 Jaimes, P. M., Bravo, A. H., Sosa, E. R., Cureño, G. I., Retama, H. A., Granados, G. G., and Becerra,
805 A. E.: Surface ozone concentration trends in Mexico City Metropolitan Area, in: Proceedings of the Air
806 and Waste Management Association's Annual Conference and Exhibition AWMA, San Antonio, Texas,
807 19-22 June 2012, 3, 2273-2284, 2012.

808 Jaimes-Palomera, M., Retama, A., Elias-Castro, G., Neria-Hernández, A., Rivera-Hernández, O., and
809 Velasco, E.: Non-methane hydrocarbons in the atmosphere of Mexico City: Results of the 2012 ozone-
810 season campaign, Atmos. Environ., 132, 258-275, doi:10.1016/j.atmosenv.2016.02.047, 2016.

811 Jenkin, M. E., and Clemitshaw, K. C.: Ozone and other secondary photochemical pollutants: chemical
812 processes governing their formation in the planetary boundary layer, Atmos. Environ., 34(16), 2499-
813 2527, doi:10.1016/S1352-2310(99)00478-1, 2000.

814 Kanda, I., Basaldud, R., Magaña, M., Retama, A., Kubo, R., and Wakamatsu, S.: Comparison of Ozone
815 Production Regimes between Two Mexican Cities: Guadalajara and Mexico City, Atmosphere, 7, 91,
816 doi:10.3390/atmos7070091, 2016.

817 Lee, Y. C., Shindell, D. T., Faluvegi, G., Wenig, M., Lam, Y. F., Ning, Z., Hao, S., and Lai, C. S.: Increase
818 of ozone concentrations, its temperature sensitivity and the precursor factor in South China, Tellus B.
819 Chem. Phys. Meteorol., 66, doi:10.3402/tellusb.v66.23455, 2014.

820 Lefohn, A. S., Shadwick, D., and Oltmans, S. J.: Characterizing changes in surface ozone levels in
821 metropolitan and rural areas in the United States for 1980-2008 and 1994-2008, Atmos. Environ, 44,
822 5199−5210, doi: 10.1016/j.atmosenv.2010.08.049, 2010.

823 Lei, W., de Foy, B., Zavala, M., Volkamer, R., and Molina, L. T.: Characterizing ozone production in the
824 Mexico City Metropolitan Area: a case study using a chemical transport model, Atmos. Chem. Phys., 7,
825 1347-1366, doi:10.5194/acp-7-1347-2007, 2007.

826 Lelieveld, J., Evans, J. S., Fnais, M., Giannadaki, D., and Pozzer, A.: The contribution of outdoor air
827 pollution sources to premature mortality on a global scale, Nature Letts., 15371,
828 doi:10.1038/nature15371, 2015.

829 Menchaca-Torre, H. L., Mercado-Hernández, R., and Mendoza-Domínguez, A.: Diurnal and seasonal
830 variation of volatile organic compounds in the atmosphere of Monterrey, Mexico, Atmos. Poll. Res., 6,
831 1073-1081, doi:10.1016/j.apr.2015.06.004, 2015.

832 Molina, M. J., and Molina, L. T.: Megacities and atmospheric pollution, J. Air Waste Manage., 54, 644-
833 680, doi:10.1080/10473289.2004.10470936, 2004.

834 Monks, P. S.: A review of the observations and origins of the spring ozone maximum, Atmos. Environ.,
835 34, 3545-3561, doi:10.1016/S1352-2310(00)00129-1, 2000.

836 Monks, P. S., Archibald, A. T., Colette, A., Cooper, O., Coyle, M., Derwent, R., Fowler, D., Granier, C.,
837 Law, K. S., Mills, G. E., Stevenson, D. S., Tarasova, O., Thouret, V., von Schneidemesser, E.,
838 Sommariva, R., Wild, O., and Williams, M. L.: Tropospheric ozone and its precursors from the urban to
839 the global scale from air quality to short-lived climate forcer, Atmos. Chem. Phys., 15, 8889-8973,
840 doi:10.5194/acp-15-8889-2015, 2015.

841 Parrish, D. D., Millet, D. B., and Goldstein, A. H.: Increasing ozone in marine boundary layer inflow at
842 the west coasts of North America and Europe, Atmos. Chem. Phys., 9, 1303-1323, doi:10.5194/acp-9-
843 1303-2009, 2009.

844 Parrish, D. D., Singh, H. B., Molina, L., and Madronich, S.: Air quality progress in North American
845 megacities: A review, Atmos. Environ., 45, 7015-7025, doi:10.1016/j.atmosenv.2011.09.039, 2011.

846 PICCA (Programa integral contra la contaminación atmosférica de la zona metropolitana de la Ciudad
847 de México), Mexico City Local Government, available at: http://centro.paot.org.mx/documentos/
848 varios/prog_inte_atmosferica.pdf, last Access: 28 April 2017, 1990

ProAire-MMA (Programa de Gestión para Mejorar la Calidad del Aire del Área Metropolitana de Monterrey 2008-2012), SEMARNAT, Gobierno del estado de Nuevo León, available at: http://www.semarnat.gob.mx/archivosanteriores/temas/gestionambiental/calidaddelaire/Documents/Calidad%20del%20aire/Proaires/ProAires_Vigentes/6_ProAire%20AMM%202008-2012.pdf, last access: 22 May 2016, 2008.

ProAire-MCMA (Programa para Mejorar la Calidad del Aire de la Zona Metropolitana del Valle de México 2002-2010), Mexico City Local Government-State of Mexico Government, available at: http://www.gob.mx/cms/uploads/attachment/file/69312/11_ProAire_ZMVM_2002-2010.pdf, last access: 28 April, 2017, 2001.

ProAire-MCMA (Programa para Mejorar la Calidad del Aire de la Zona Metropolitana del Valle de México 2002-2010), Mexico City Local Government-State of Mexico Government, available at: http://www.aire.cdmx.gob.mx/descargas/publicaciones/flippingbook/proaire2011-2020/#p=1, last access: 28 April 2017, 2011

Pugliese, S. C., Murphy, J. G., Geddes, J. A., and Wang, J. M.: The impacts of precursor reduction and meteorology on ground-level ozone in the Greater Toronto Area, Atmos. Chem. Phys., 14, 8197-8207, doi:10.5194/acp-14-8197-2014, 2014.

Pusede, S. E., and Cohen, R. C. On the observed response of ozone to NO_x and VOC reactivity reductions in San Joaquin Valley California 1995–present, Atmos. Chem. Phys., 12, 8323-8339, doi:10.5194/acp-12-8323-2012, 2012.

Pusede, S. E., Steiner, A. L., and Cohen, R.C.: Temperature and recent trends in the chemistry of continental surface ozone, Chem. Rev., 115, 3898-3918, doi: 10.1021/cr5006815, 2015.

R Core Team: R: a Language and Environment for Statistical Computing, R Foundation for Statistical Computing, Vienna, Austria, ISBN 3-900051-07-0, 2013, available at: www.R-project.org, last access: 23 May 2016, 2013.

Radian (International): Mexico Emissions Inventory Program Manuals (Vol. II-VI), available at: https://www3.epa.gov/ttncatc1/cica/other3_s.html, last access: 15 Jan 2017, 2000.

Reinsel, G. C.: Elements of Multivariate Time Series Analysis. Springer-Verlag, New York, USA, 2nd Edition, 1997.

Revell, L. E., Tummon, F., Stenke, A., Sukhodolov, T., Coulon, A., Rozanov, E., Garny, H., Grewe, V. and Peter, T.: Drivers of the tropospheric ozone budget throughout the 21st century under the medium-high climate scenario RCP 6.0, Atmos. Chem. Phys., 15, 5887-5902, doi:10.5194/acp-15-5887-2015, 2015.

Rodríguez, S., Huerta, G., and Reyes, H.: A study of trends for Mexico City ozone extremes: 2001-2014, Atmosfera, 29, 107-120, doi:10.20937/ATM.2016.29.02.01, 2016.

Russell, A. R., Valin, L. C., and Cohen, R. C.: Trends in OMI NO_2 observations over the United States: effects of emission control technology and the economic recession, Atmos. Chem. Phys., 12, 12197-12209, doi:10.5194/acp-12-12197-2012, 2012.

Salmi, T., Määttä, A., Anttila, P., Ruoho-Airola, T. and Amnell, T.: Detecting trends of annual values of atmospheric pollutants by the Mann-Kendall test and Sen's slope estimates – the Excel template application MAKESENS, Publications on Air Quality Report code FMI-AQ-31, Helsinki, Finland, 31, 1-35, 2002.

Sather, M.E. and Cavender, K.: Trends analyses of 30 years of ambient 8 hour ozone and precursor monitoring data in the South Central US: progress and challenges, Environ. Sci. Proc. Imp., 18, 819-831. 2016.

Schultz, M., and Rast, S.: REanalysis of the TROpospheric chemical composition over the past 40 years, Emission Data Sets and Methodologies for Estimating Emissions, Work Package 1, Deliverable D1-6,

available at: http://retro-archive.iek.fz-juelich.de/data/documents/reports/D1-6_final.pdf, last access: 14 Jul 2016, 2007.

SDS (Secretaria de Desarrollo Sustentable), Inventario de emisiones del Área Metropolitana de Monterrey 2013, personal communication, Monterrey, N.L. México, 4 Sep 2015.

SDS (Secretaria de Desarrollo Sustentable): Sistema Integral de Monitoreo Ambiental, available at: http://aire.nl.gob.mx/, last access: 21 May 2016, 2016.

SEDEMA (Secretaria del Medio Ambiente): INVENTARIO de Emisiones a la Atmosfera en la ZMVM 1996, available at: http://www.sedema.df.gob.mx/flippingbook/inventario-emisiones-1996/#p=1, last access: 20 May 2016, 1999.

SEDEMA (Secretaria del Medio Ambiente): Inventario de Emisiones Zona Metropolitana del Valle de Mexico 1998, available at: http://www.sedema.df.gob.mx/flippingbook/inventario-emisiones-zmvm1998/#p=75, last access: 20 May 2016, 2001.

SEDEMA (Secretaria del Medio Ambiente): Inventario de emisiones a la Atmosfera Zona Metropolitana del Valle de Mexico 2000, available at: http://www.sedema.df.gob.mx/ flippingbook/inventario-emisiones-zmvm2000/, last access: 20 May 2016, 2003.

SEDEMA (Secretaria del Medio Ambiente): Inventario de emisiones de la Zona Metropolitana del Valle de Mexico 2002, available at: http://www.sedema.df.gob.mx/flippingbook/inventario-emisiones-zmvm-criterio2004/#p=1, last access: 20 May 2016, 2004.

SEDEMA (Secretaria del Medio Ambiente): Inventario de Emisiones Zona Metropolitana del Valle de Mexico 2004, available at: http://www.sedema.df.gob.mx/flippingbook/inventario-emisiones-zmvm-criterio2004/#p=1, last access: 20 May 2016, 2006.

SEDEMA (Secretaria del Medio Ambiente): Inventario de Emisiones de Contaminantes Criterio 2006, available at: http://www.sedema.df.gob.mx/flippingbook/inventario-emisiones-zmvm-criterio2006/#p=1, last access: 20 May 2016, 2008.

SEDEMA (Secretaria del Medio Ambiente): Inventario de emisiones de contaminantes criterio de la ZMVM 2008, available at: http://www.sedema.df.gob.mx/flippingbook/inventario-emisiones-zmvm-criterio2008/#p=1, last access: 20 May 2016, 2010.

SEDEMA (Secretaria del Medio Ambiente): Inventario de emisiones de la Zona Metroplitiana del Valle de Mexico contaminantes criterio 2010, available at: http://www.sedema.df.gob.mx/flippingbook/inventario-em1isiones-zmvm-criterio-2010/#p=6, last access: 20 May 2016, 2012.

SEDEMA (Secretaria del Medio Ambiente): Inventario de Emisiones Contaminantes y de efecto invernadero, available at: http://www.sedema.df.gob.mx/flippingbook/inventario-emisioneszmvm2012/, last access: 20 May 2016, 2014.

SEDEMA (Secretaria del Medio Ambiente de la Ciudad de Mexico): Sistema de Monitoreo Atmosférico, available at: http://www.aire.df.gob.mx/default.php, last access: 21 May 2016, 2016a.

SEDEMA (Secretaria del Medio Ambiente de la Ciudad de Mexico): Inventario de Emisiones de la CDMX 2014 Contaminantes Criterio Tóxicos y de Efecto Invernadero, available at: http://www.aire.cdmx.gob.mx/descargas/publicaciones/flippingbook/inventario-emisiones-cdmx2014-2/, last Access: 10 Jan 2017, 2016b.

SEMARNAT (Secretaria del Medio Ambiente y Recursos Naturales): NOM-041 (NORMA OFICIAL MEXICANA, QUE ESTABLECE LOS LIMITES MAXIMOS PERMISIBLES DE EMISION DE GASES CONTAMINANTES PROVENIENTES DEL ESCAPE DE LOS VEHICULOS AUTOMOTORES EN CIRCULACION QUE USAN GASOLINA COMO COMBUSTIBLE), Diario Oficial de la Federación, 1993.

SEMARNAT (Secretaria del Medio Ambiente y Recursos Naturales): NOM-042 (NORMA OFICIAL MEXICANA QUE ESTABLECE LOS LIMITES MAXIMOS PERMISIBLES DE EMISION DE HIDROCARBUROS TOTALES O NO METANO, MONOXIDO DE CARBONO, OXIDOS DE NITROGENO Y PARTICULAS PROVENIENTES DEL ESCAPE DE LOS VEHICULOS AUTOMOTORES NUEVOS CUYO PESO BRUTO VEHICULAR NO EXCEDA LOS 3,857 KILOGRAMOS, QUE USAN GASOLINA, GAS LICUADO DE PETROLEO, GAS NATURAL Y DIESEL, ASI COMO DE LAS EMISIONES DE HIDROCARBUROS EVAPORATIVOS PROVENIENTES DEL SISTEMA DE COMBUSTIBLE DE DICHOS VEHICULOS), Diario Oficial de la Federación, 1993.

SEMARNAT (Secretaria del Medio Ambiente y Recursos Naturales): Inventario Nacional de Emisiones 1999, México, D.F., available at: http://www.inecc.gob.mx/dica/548-calaire-inem-1999, last access: 20 May 2016, 2006.

SEMARNAT (Secretaria del Medio Ambiente y Recursos Naturales): Inventario Nacional de Emisiones 2005, México, D.F., available at: http://sinea.semarnat.gob.mx/sinae.php?process=UkVQT1JURUFET1I=&categ=1, last access: 22 May 2016, 2011.

SEMARNAT (Secretaria del Medio Ambiente y Recursos Naturales): Inventario Nacional de Emisiones 2008, México, D.F., available at: http://sinea.semarnat.gob.mx/ sinae.php?process=UkVQT1JURUFET1I=&categ=14, last access: 22 May 2016, 2014.

SEMARNAT (Secretaria del Medio Ambiente y Recursos Naturales): Informe Nacional de calidad del aire 2014, México, D.F., available at: http://inecc.gob.mx/descargas/calaire/2015_Informe_nacional_calidad_aire_2014_Final.pdf, last access: 15 Dec 2016, 2015.

SENER (Secretaria de Energia): Estadísticas Energéticas Nacionales, México, available at: http://sie.energia.gob.mx/bdiController.do?action=temas, last access: 4 November 2015, 2015.

Sicard, P., Serra, R., and Rossello, P.: Spatiotemporal trends in ground-level ozone concentrations and metrics in France over the time period 1999-2012, Environ. Res., 149, 122-144, doi:10.1016/j.envres.2016.05.014, 2016

Sierra, A., Vanoye, A. Y., and Mendoza, A.: Ozone sensitivity to its precursor emissions in northeastern Mexico for a summer air pollution episode, J. Air Waste Manage., 63, 1221-1233, doi:10.1080/10962247.2013.813875, 2013.

Simon, H., Reff, A., Wells, B., Xing, J., and Frank, N.: Ozone trends across the United States over a period of decreasing NO_x and VOC emissions, Environ. Sci. Tech., 49, 186-195. doi:10.1021/es504514z, 2015.

SMN (Servicio Meteorológico Nacional), available at: http://smn.cna.gob.mx/es/, last access: 21 May 2016.

Staehelin, J., and Schmid, W.: Trend analysis of tropospheric ozone concentrations utilizing the 20-year data set of ozone balloon soundings over Payerne (Switzerland), Atmos. Environ., 25, 1739-1749, doi:10.1016/0960-1686(91)90258-9, 1991.

Stein, A. F., Draxler, R. R., Rolph, G. D., Stunder, B. J. B., Cohen, M. D., and Ngan, F.: NOAA'S HYSPLIT atmospheric transport and dispersion modelling system. Am. Meteorol. Soc., 96, 2059-2077, doi:10.1175/BAMS-D-14-00110.1, 2015.

Stephens, S., Madronich, S., Wu, F., Olson, J. B., Ramos, R., Retama, A., and Muñoz, R.: Weekly patterns of México City's surface concentrations of CO, NO_x, PM_{10} and O_3 during 1986-2007, Atmos. Chem. Phys., 8, 5313-5325, doi:10.5194/acp-8-5313-2008, 2008.

Stevenson, D. S., Dentener, F. J., Schultz, M. G., Ellingsen, K., van Noije, T. P. C., Wild, O., Zeng, G., Amann, M., Atherton, C. S., Bell, N., Bergmann, D. J., Bey, I., Butler, T., Cofala, J., Collins, W. J., Derwent, R. G., Doherty, R. M., Drevet, J., Eskes, H. J., Fiore, A. M., Gauss, M., Hauglustaine, D. A., Horowitz, L. W., Isaksen, I. S .A., Krol, M. C., Lamarque, J.-., Lawrence, M. G., Montanaro, V., Müller, J.-., Pitari, G., Prather, M. J., Pyle, J. A., Rast, S., Rodriguez, J. M., Sanderson, M. G., Savage, N. H.,

Shindell, D. T., Strahan, S. E., Sudo, K., and Szopa, S.: Multimodel ensemble simulations of present-day and near-future tropospheric ozone. J. Geophys. Res., D08301, doi: 10.1029/2005JD006338, 2006.

Strode, S. A., Rodriguez, J. M., Logan, J. A., Cooper, O. R., Witte, J. C., Lamsal, L. N., Damon, M., Van Aartsen, B., Steenrod, S. D., and Strahan, S. E.: Trends and variability in surface ozone over the United States, J. Geophys. Res., 120, 9020-9042, doi:10.1002/2014JD022784, 2015.

Tiwari, A. K., Suresh, K. G., Arouri, M., and Teulon, F.: Causality between consumer price and producer price: Evidence from Mexico, Econ. Model., 36, 432-440, doi:10.1016/j.econmod.2013.09.050, 2014.

Torres-Jardon, R., García-Reynoso, J. A., Jazcilevich, A., Ruiz-Suárez, L. G., and Keener, T. C.: Assessment of the ozone-nitrogen oxide-volatile organic compound sensitivity of Mexico City through an indicator-based approach: measurements and numerical simulations comparison, J. Air Waste Manag. Assoc., 59, 1155-1172, doi:10.3155/1047-3289.59.10.1155, 2009.

VanCuren, R.: Transport aloft drives peak ozone in the Mojave Desert, Atmos. Environ., 109, 331-341, doi: 10.1016/j.atmosenv.2014.09.057, 2015.

Vingarzan, R.: A review of surface ozone background levels and trends, Atmos. Environ., 38, 3431-3442, doi:10.1016/j.atmosenv.2004.03.030, 2004.

Velasco, E., Lamb, B., Westberg, H., Allwine, E., Sosa, G., Arriaga-Colina, J. L., Jobson, B. T., Alexander, M. L., Prazeller, P., Knighton, W. B., Rogers, T. M., Grutter, M., Herndon, S. C., Kolb, C. E., Zavala, M., de Foy, B., Volkamer, R., Molina, L. T., and Molina, M. J.: Distribution, magnitudes, reactivities, ratios and diurnal patterns of volatile organic compounds in the Valley of Mexico during the MCMA 2002 & 2003 field campaigns, Atmos. Chem. Phys., 7, 329-353, doi:10.5194/acp-7-329-2007, 2007.

Wang, Y., Konopka, P., Liu, Y., Chen, H., Müller, R., Plöger, F., Riese, M., Cai, Z., and Lü, D.: Tropospheric ozone trend over Beijing from 2002-2010: Ozonesonde measurements and modeling analysis, Atmos. Chem. Phys., 12, 8389-8399, doi:10.5194/acp-12-8389-2012, 2012.

Wilson, R. C., Fleming, Z. L., Monks, P. S., Clain, G., Henne, S., Konovalov, I. B., Szopa, S., and Menut, L.: Have primary emission reduction measures reduced ozone across Europe? An analysis of European rural background ozone trends 1996-2005, Atmos. Chem. Phys., 12, 437-454, doi:10.5194/acp-12-437-2012, 2012.

Wolff, G. T., Kahlbaum, D. F., and Heuss, J. M.: The vanishing ozone weekday/weekend effect, J. Air Waste Manage., 63, 292-299, doi:10.1080/10962247.2012.749312, 2013.

World Health Organization: Ambient (outdoor) air quality and health, 2014 update, http://www.who.int/mediacentre/factsheets/fs313/en/, last access: 21 May 2016.

Xing, J., Pleim, J., Mathur, R., Pouliot, G., Hogrefe, C., Gan, C.-M., and Wei, C.: Historical gaseous and primary aerosol emissions in the United States from 1990 to 2010, Atmos. Chem. Phys., 13, 7531-7549, doi:10.5194/acp-13-7531-2013, 2013.

Xu, X., Lin, W., Wang, T., Yan, P., Tang, J., Meng, Z., and Wang, Y.: Long-term trend of surface ozone at a regional background station in eastern China 1991-2006: Enhanced variability, Atmos. Chem. Phys., 8, 2595-2607, doi:10.5194/acp-8-2595-2008, 2008.

Zellweger, C., Hüglin, C., Klausen, J., Steinbacher, M., Vollmer, M., and Buchmann, B.: Inter-comparison of four different carbon monoxide measurement techniques and evaluation of the long-term carbon monoxide time series of Jungfraujoch, Atmos. Chem. Phys., 9, 3491-3503, doi:10.5194/acp-9-3491-2009, 2009.

Zheng, J., Swall, J. L., Cox, W. M., and Davis, J. M. Interannual variation in meteorologically adjusted ozone levels in the eastern United States: A comparison of two approaches, Atmos. Environ., 41, 705-716, doi:10.1016/j.atmosenv.2006.09.010, 2007.

Table 1. Air quality limit values stated in Mexican legislation.

Pollutant	Mexican Official Standard	Limit value*
O_3 (ppb)	NOM-020-SSA1-1993	110 (1-h), 80 (8-h)[a,b]
	NOM-020-SSA1-2014	95 (1-h) , 70 (8-h)[a,b]
PM_{10} ($\mu g\ m^{-3}$)	NOM-025-SSA1-1993	75 (24-h), 40 (1-yr)
	NOM-025-SSA1-2014	50 (24h), 35 (1-yr)
$PM_{2.5}$ ($\mu g\ m^{-3}$)	NOM-025-SSA1-1993	45 (24-h), 12 (1-yr)
	NOM-025-SSA1-2014	30 (24-h), 10 (1-yr)
CO (ppm)	NOM-02-SSA1-1993	11 (8-h)[b]
NO_2 (ppm)	NOM-023-SSA1 -1993	0.21 (1-h)

*Average period.
[a]Not to be exceeded more than 4 times in a calendar year.
[b]Running average.

Table 2. Site description, location and instrumentation used during 1993 to 2014 within the MMA.

Site	Code	Location	Elevation (m a.s.l.)	Site description
Guadalupe	GPE	25° 40.110' N, 100° 14.907' W	492	Urban background site in the La Pastora park, surrounded by a highly populated area, 450 m from Pablo Rivas Rd.
San Nicolas	SNN	25° 44.727' N, 100° 15.301' W	476	Urban site surrounded by a large number of industries and residential areas, 450 m from Juan Diego Diaz de Beriagna Rd.
Obispado	OBI	25° 40.561' N, 100° 20.314' W	560	Urban site near the city centre of MMA, 250 m from Jose Eleuterio González Rd. and 250 m from Antonio L. Rodríguez Rd.
San Bernabe	SNB	25° 45.415' N, 100° 21.949' W	571	Urban site in a residential area downwind of an industrial area with high traffic volume, 140 m from Aztlan Rd.
Santa Catarina	STA	25° 40.542' N, 100° 27.901' W	679	Urban site downwind of industrial sources, 200 m from Manuel Ordoñez Rd.

Table 3. Results for O_3 and O_X long-term trends expressed in ppb yr^{-1} for 1993-2014 at the 5 sites within the MMA by season.

Site	Period	Ozone (O_3)			Odd oxygen ($O_x = O_3 + NO_2$)		
		ppb yr^{-1}	% yr^{-1}	Significance	ppb yr^{-1}	% yr^{-1}	Significance
GPE	Annual	0.21	0.78	*	0.31	0.80	**
	Spring	0.24	0.73	*	0.32	0.69	*
	Summer	0.30	1.16	*	0.38	1.18	*
	Autumn	0.14	0.53		0.25	0.62	
	Winter	0.12	0.53		0.14	0.33	*
SNN	Annual	0.33	1.40	***	0.45	1.25	*
	Spring	0.39	1.38	*	0.49	1.22	*
	Summer	0.47	2.24	*	0.58	1.87	***
	Autumn	0.41	1.96	*	0.65	1.94	*
	Winter	0.14	0.68		0.23	0.58	+
OBI	Annual	0.30	1.29	*	-0.17	-0.35	
	Spring	0.43	1.56	*	0.02	0.03	*
	Summer	0.26	0.98	*	-0.04	-0.09	
	Autumn	0.29	1.33	+	-0.66	-1.15	
	Winter	0.25	1.46		-0.28	-0.53	
SNB	Annual	0.19	0.65	+	0.61	1.66	**
	Spring	0.37	1.07	+	0.67	1.65	+
	Summer	0.31	1.06	***	0.66	2.17	***
	Autumn	0.19	0.64		0.60	1.61	+
	Winter	0.02	0.07		0.47	1.12	+
STA	Annual	0.01	0.01		-0.15	-0.28	
	Spring	-0.04	-0.11		-0.01	-0.02	
	Summer	0.09	0.28		0.13	0.27	
	Autumn	0.00	0.00		-0.22	-0.41	
	Winter	-0.09	-0.43		-0.63	-1.15	*

+Level of significance $p < 0.1$.
*Level of significance $p < 0.05$.
**Level of significance $p < 0.001$.
***Level of significance $p < 0.001$.

Table 4. Results for O_3 and O_X long-term trends by season expressed in ppb yr^{-1} during 1993-2014 for the MCMA and MMA, and during 1996-2014 for the GMA.

Urban area	Period	Ozone (O_3)			Odd oxygen ($O_3 + NO_2$)		
		ppb yr^{-1}	% yr^{-1}	Significance	ppb yr^{-1}	% yr^{-1}	Significance
MCMA	Annual	-1.15	-2.04	***	-1.87	-1.94	***
	Spring	-0.97	-1.53	***	-1.77	-1.71	***
	Summer	-0.97	-1.88	***	-1.44	-1.67	***
	Autumn	-1.12	-2.20	***	-1.89	-2.15	***
	Winter	-1.62	-2.64	***	-2.47	-2.27	***
GMA	Annual	-0.29	-0.81		-1.46	-1.85	+
	Spring	-0.26	-0.57		-1.89	-2.07	*
	Summer	-0.10	-0.32		-1.43	-1.89	*
	Autumn	-0.09	0.33		-1.40	-1.97	*
	Winter	-0.34	-1.01		-1.74	-2.08	***
MMA	Annual	0.22	0.84	**	0.13	0.30	
	Spring	0.32	1.04	**	0.29	0.63	
	Summer	0.27	0.99	***	0.28	0.72	***
	Autumn	0.25	1.03		0.13	0.31	
	Winter	0.10	0.45		0.01	-0.01	

+Level of significance $p < 0.1$.
*Level of significance $p < 0.05$.
**Level of significance $p < 0.001$.
***Level of significance $p < 0.001$.

Table 5. Results for O_3 daily maxima long-term trends by season in ppb yr^{-1} during 1993-2014 at the 5 sites within the MMA.

Site	Period	Ozone (O_3)		
		ppb yr^{-1}	% yr^{-1}	Significance
GPE	Annual	0.45	1.02	**
	Spring	0.48	0.94	**
	Summer	0.64	1.50	*
	Autumn	0.35	0.74	
	Winter	0.26	0.63	
SNN	Annual	0.79	2.13	***
	Spring	0.87	2.01	***
	Summer	0.85	2.42	***
	Autumn	0.93	2.73	*
	Winter	0.44	1.29	
OBI	Annual	0.65	1.51	*
	Spring	0.78	1.62	**
	Summer	0.53	1.10	*
	Autumn	0.75	1.77	
	Winter	0.21	0.55	
SNB	Annual	0.40	0.80	***
	Spring	0.85	1.58	***
	Summer	0.67	1.36	***
	Autumn	0.52	1.05	*
	Winter	0.05	0.10	
STA	Annual	0.01	-0.01	
	Spring	-0.05	-0.09	
	Summer	0.22	0.35	
	Autumn	-0.07	-0.12	
	Winter	-0.35	-0.75	+

+Level of significance $p < 0.1$.
*Level of significance $p < 0.05$.
**Level of significance $p < 0.001$.
***Level of significance $p < 0.001$.

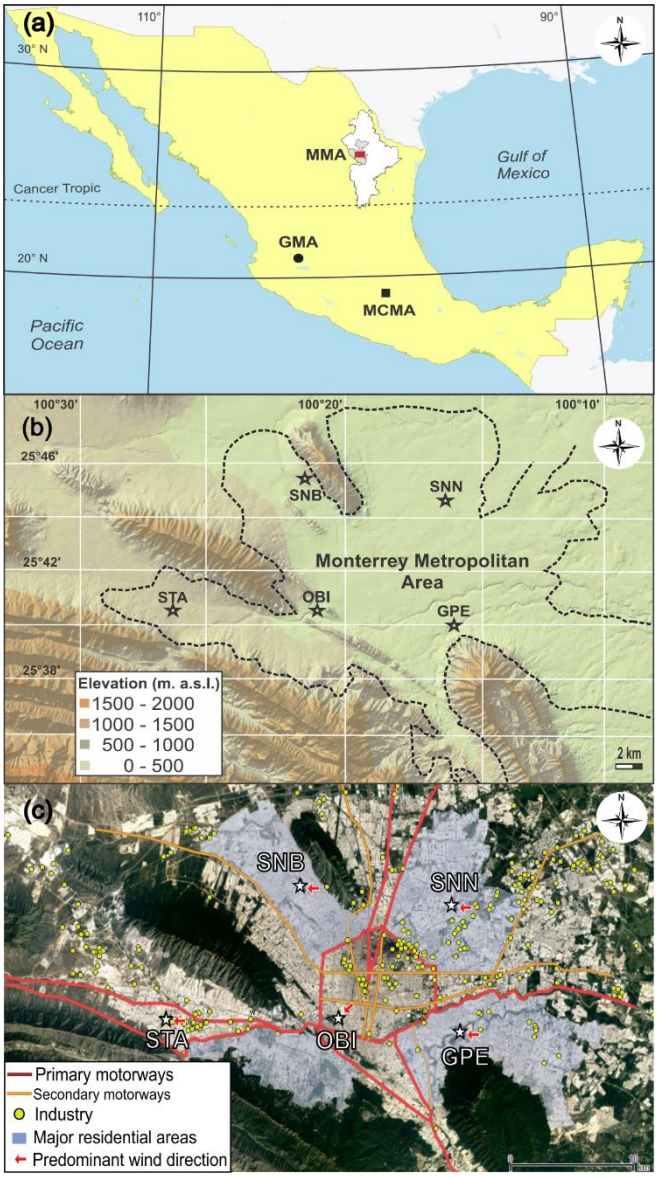

Fig. 1(a). The MMA, MCMA and GMA in the national context. **(b).** Topography of the MMA and distribution of the 5 monitoring sites over the area. **(c).** The 5 monitoring sites in relation to primary and secondary motorways, industries and major residential areas. The red arrows show the predominant wind direction at each site during 1993 to 2014.

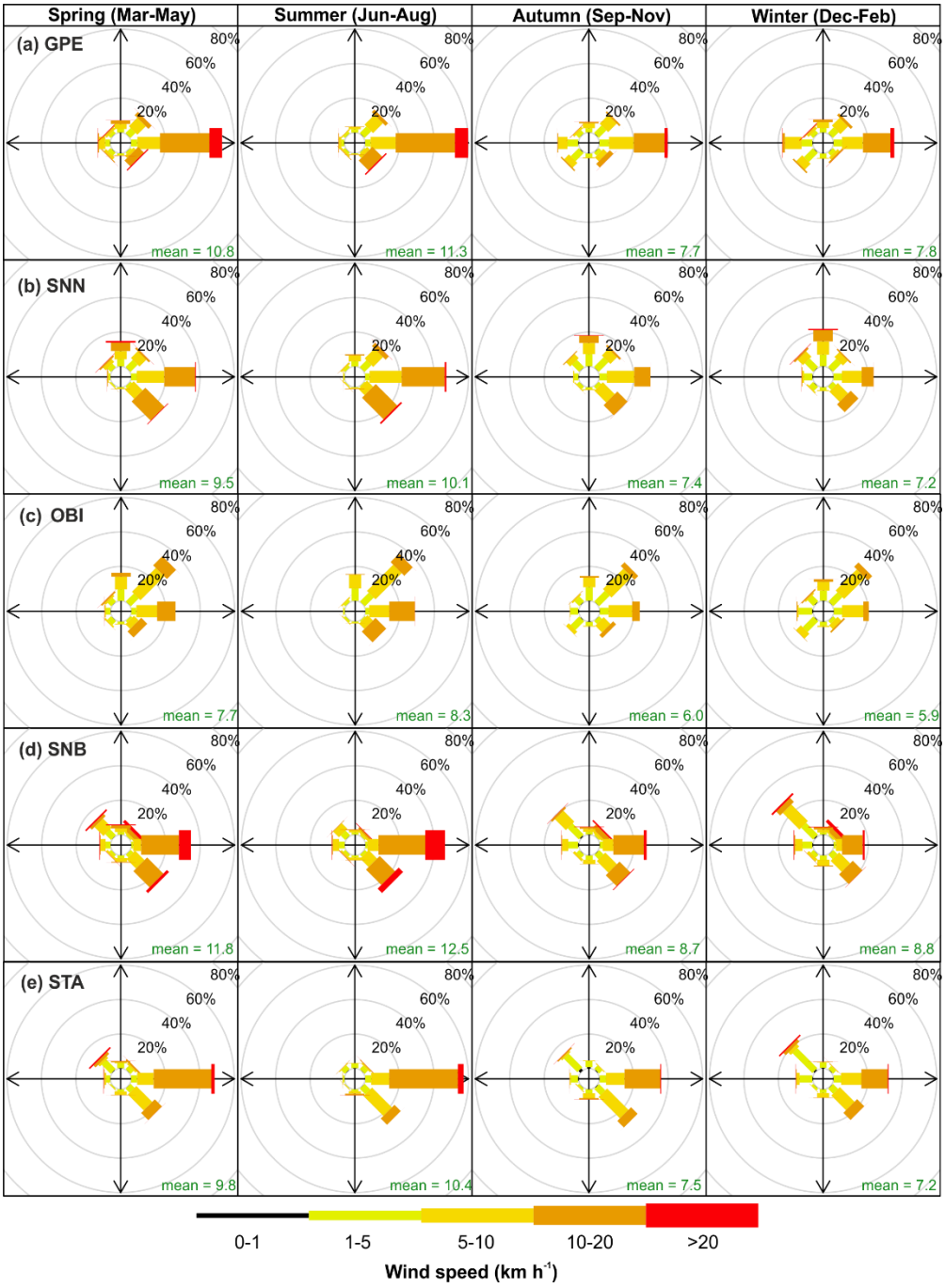

Fig. 2. Frequency of counts of measured wind direction occurrence by season and site within the MMA during 1993-2014.

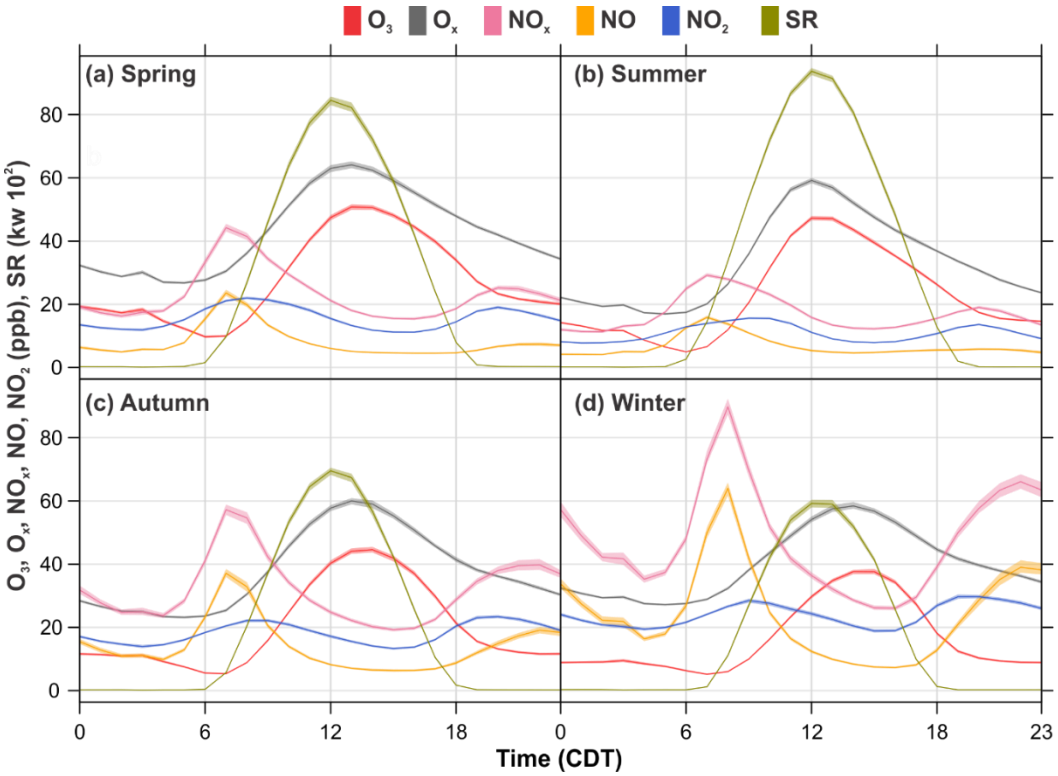

Fig. 3. Seasonal average daily profiles for O_3, O_X, NO_X, NO, NO_2 and SR within the MMA during 1993-2014. The shading shows the 95 % confidence intervals of the average.

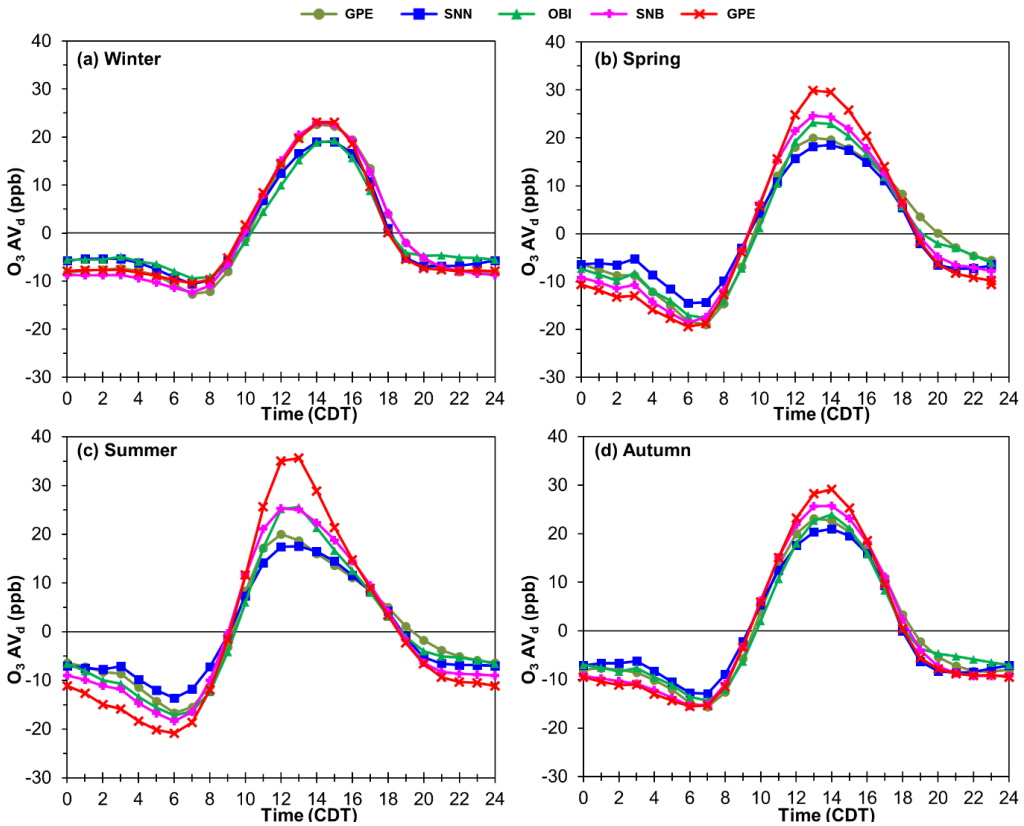

Fig. 4. Seasonal O_3 de-trended daily profiles within the MMA during 1993-2014. De-trended O_3 daily cycles were constructed by subtracting daily averages from hourly averages to remove the impact of long-term trends.

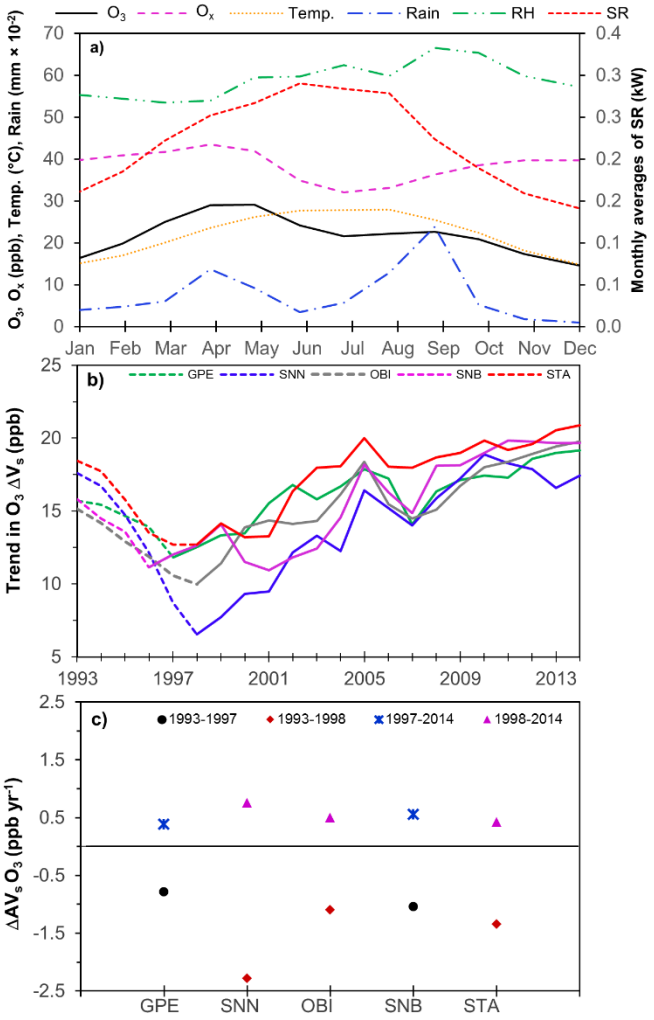

1119

1120 **Fig. 5a).** Annual cycles of O_3, temperature, rainfall, RH and SR constructed by averaging records from
1121 1993 to 2014 for a 1-year period. **b).** Trends in AV_s of O_3 recorded at the 5 monitoring sites within the
1122 MMA from 1993 to 2014. The decline in AV_s observed is due to the economic crisis experienced in
1123 Mexico during 1994-1996, followed by persistent increases in AV_s since 1998. **c).** Annual rates of change
1124 in O_3 AV_s by site, before and after the 1994-1996 economic crisis.
1125

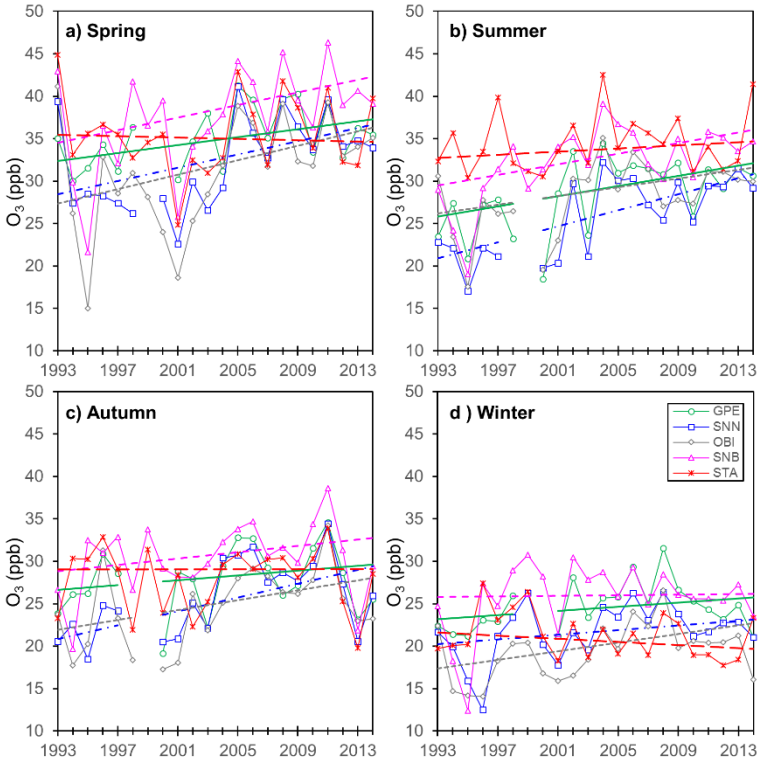

Fig. 6. Seasonal trends of O_3 within the MMA during 1993-2014. Each data point represents the average of the 3-month period that defines the season. The continuous lines show the Sen trend.

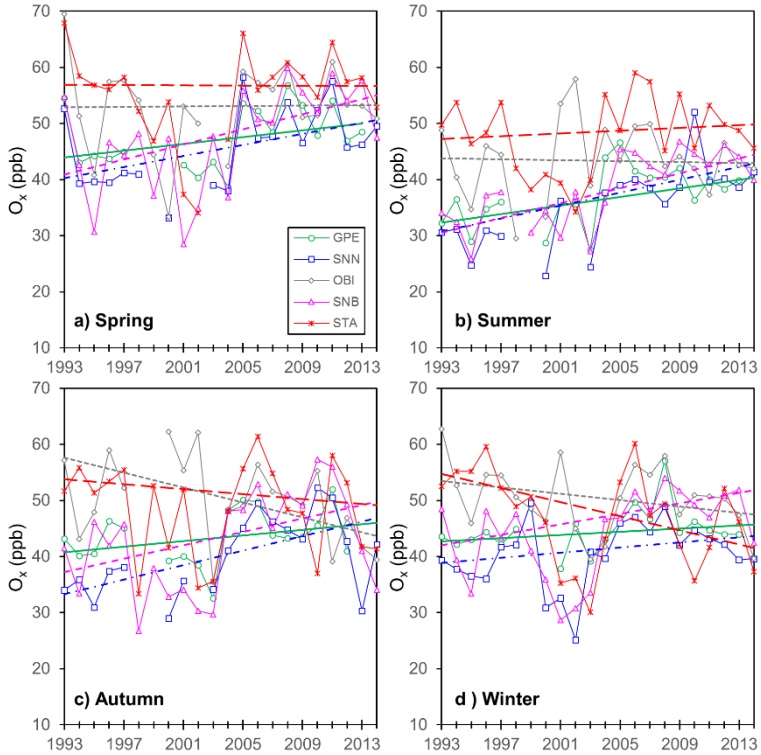

Fig. 7. Seasonal trends of O_X within the MMA during 1993-2014. Each data point represents the average of the 3-month period that defines the season. The continuous lines show the Sen trend.

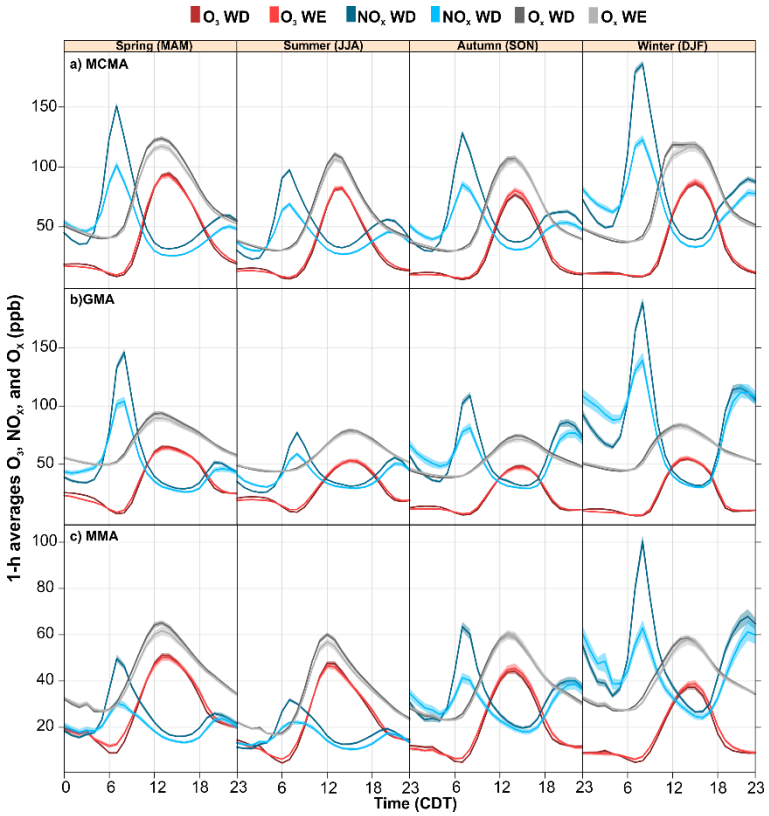

Fig. 8. Seasonal average diurnal cycles of O_3, O_X and NO_X during 1993-2014 for the MCMA and the MMA, and between 1996-2014 for the GMA. The shading shows the 95% confidence intervals of the average, calculated through bootstrap resampling (Carslaw, 2015).

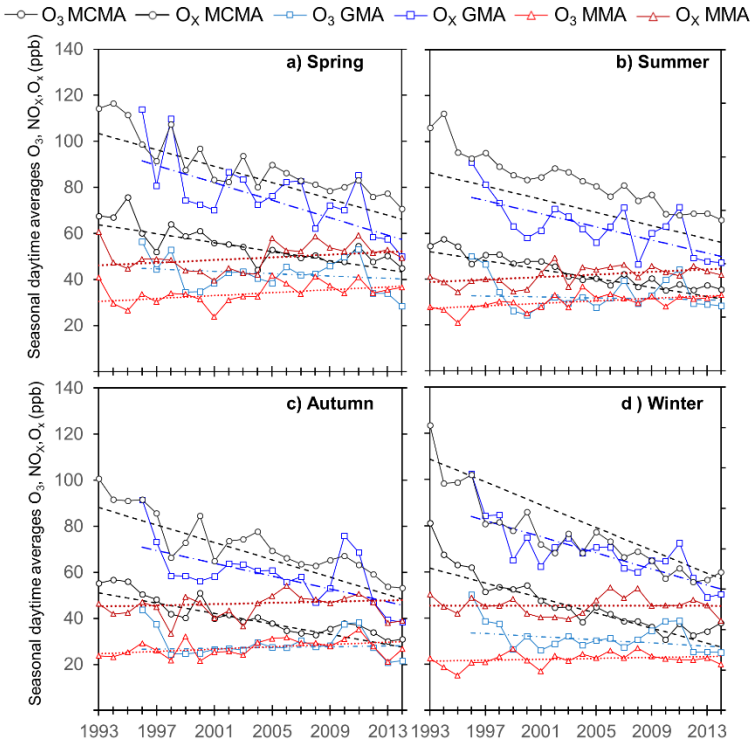

Fig. 9. Seasonal trends in O_3 and O_x for the MCMA and MMA during 1993-2014, and for the GMA during 1996-2014. Each data point represents the average of the 3-month period that defines the season. The dashed lines show the Sen trend.

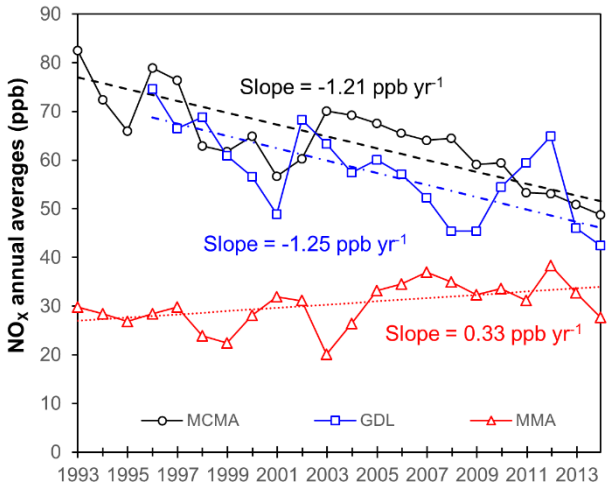

Fig. 10. Trends for NO_X at the MCMA and MMA during 1993-2014, and at the GMA during 1996-2014. The dashed lines represent the Sen slopes. All trends are statistically significant at $p<0.05$.

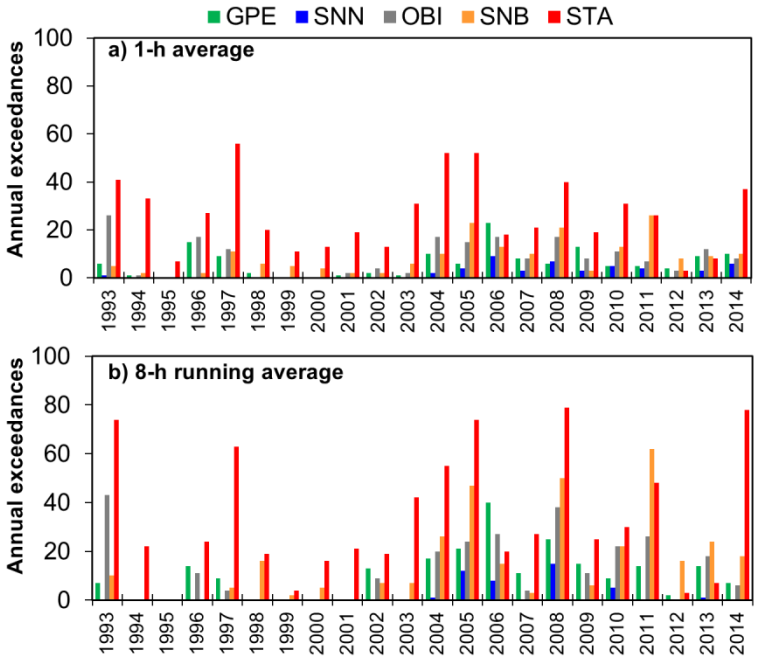

Fig. 11. Annual exceedances of the O_3 NOM for 1-h averages (110 ppb) and 8-h running averages (80 ppb) at the 5 monitoring sites within the MMA from 1993 to 2014.

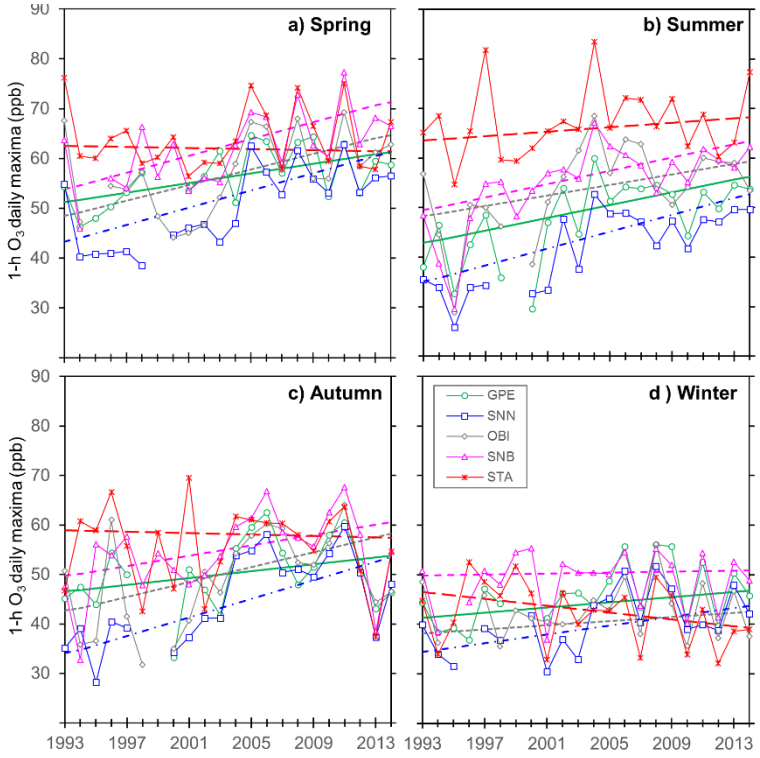

Fig. 12. Seasonal trends in 1-h O_3 daily maxima at the MMA during 1993-2014. Each data point represents the average of the 3-month period that defines the season. The dashed lines show the Sen trend.

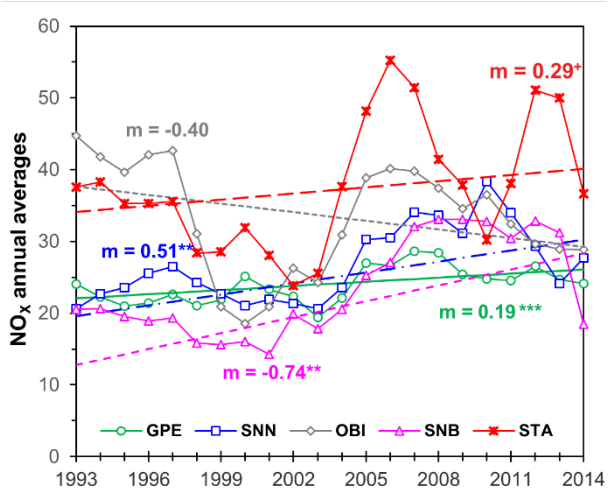

Fig. 13. Long-term trends for NO_X at the 5 monitoring sites within the MMA during 1993-2014. The dashed lines represent the Sen slopes. Annual NO_X rates of change are described as m for slope and expressed in units of ppb yr^{-1}. Levels of confidence are represented as $^+ = p<0.1$, * = $p<0.05$, ** = $p<0.001$, *** = $p<0.001$.